# Development of Photonic Crystal Hydrogel Sensors For Organophosphates and Ammonia

By

Jeremy P. Walker

B.A. Colgate University, 2001

Submitted to the Graduate Faculty of
Arts and Sciences in partial fulfillment
of the requirements for the degree of
Doctor of Philosophy

University of Pittsburgh
November 30th, 2006

UNIVERSITY OF PITTSBURGH

_____

FACULTY OF ARTS AND SCIENCES

This dissertation was presented

By

<u>Jeremy P. Walker</u>

It was defended on

<u>November 30<sup>th</sup>, 2006</u>

and approved by

_____Adrian C. Michael

_____Stéphane Petoud

_____David N. Finegold

_____Alexander Star

_____

_____Sanford A. Asher
Committee Chairperson

# Development of Photonic Crystal Hydrogel Sensors
## For Organophosphates and Ammonia

Jeremy P. Walker, Ph.D.

University of Pittburgh, 2006

We developed several photonic crystal hydrogel sensors based on our Polymerized Crystalline Colloidal Array (PCCA) technology. Highly-charged colloidal particles ~ 100 nm in size self-assemble in low ionic strength solutions to form an electrostatically stabilized crystalline colloidal array (CCA). These CCA occur as either face-centered cubic (fcc) or body-centered cubic (bcc) lattice structures which Bragg diffract light in the visible, near IR and UV regions of the spectrum.

The  CCA ordering is preserved by locking it into place within polymer hydrogels, forming a polymerized crystalline colloidal array (PCCA). The Asher group utilizes the hydrogel's sensitivity for its environment to develop sensors for specific analytes by functionalizing the hydrogel backbone with molecular recognition agents which are specific for a single analyte. Analyte recognition cause volume phase transitions in the hydrogel which shrink or swell the network and changes the lattice spacing of the embedded CCA. As a result, changes in the wavelength of Bragg diffracted light correspond to the concentration of analyte present in the solution.

We developed sensors for organophosphorus (OP) nerve agents utilizing enzymes as molecular recognition agents. The first sensor utilizes the enzyme acetylcholinesterase, which irreversibly binds the OP, creating a charged species. The resulting Donnan

potential swells the hydrogel and red-shifts the diffraction proportional to the OP

concentration. The sensor functions as a dosimeter and displays ultra-trace detection

levels (4 fM) for OP species in low-ionic strength media.

The second OP sensor utilizes two recognition agents. The enzyme

organophosphorus hydrolase (OPH) and the pH-sensitive group 3-aminophenol are

attached to the hydrogel. OPH hydrolyzes OPs at basic pH and produces protons. These

protons in turn create a pH gradient inside the hydrogel which titrates the phenolates,

lowering the free-energy of mixing of the hydrogel and blue-shifting the wavelength of

Bragg diffracted light proportional to the OP concentration. The sensor is reversible,

functions in high-ionic strength media, and has a 0.2 μM OP detection limit in aqueous

media.

We also fabricated a sensor for ammonia which functions in human serum.

Phenols on the hydrogel backbone are cross-linked through reaction of ammonia with

added hypochlorite. The cross-linking causes an increase in the elastic constant of the

hydrogel which forces the gel to shrink, blue-shifting the wavelength of Bragg diffracted

light proportional to the concentration of ammonia present in solution. The sensor

functions within the clinically relevant ammonia interval with a detection limit ~ 50 μM

$NH_3$ in 1:1 serum/buffer solutions.

# Acknowledgments

I would first like to express my thanks to my research advisor, Dr. Sanford A. Asher, whose leadership style has allowed me to grow as an independent researcher and to develop critical thinking skills which are crucial for research. He has helped me to become capable of conceiving new ideas and acquiring the tools and knowledge to be a successful researcher. I have enjoyed my interactions with him personally and as a member of the group, and am very thankful to have had this research experience.

I also wish to thank all past and present members of the group for their help and for their friendship. In particular, I would like to thank Dr. Chad E. Reese for helping me acclimate to the group, Dr. Anjal Sharma for helpful advice, and Dr. Vladimir Alexeev for all of his helpful suggestions and for his friendship. I also would like to thank Dr. David Finegold for his mentorship and his levelheaded approach to science. Finally, I would like to thank my collaborator, Kyle Kimble, for the many enjoyable hours of work and discussions which have made graduate school and research a lot of fun for the past three years.

I would also like to thank the members of my committee, Dr. Adrian Michael, Dr. Stéphane Petoud, and Dr. Alexander Star, for their helpful influence and time in my thesis and also in my development as a student and scientist.

I would like to thank my parents D. Jerry and Vivian Walker for their sacrifice to send me to school and for giving me an initial opportunity to obtain an education at several very prestigious academic institutions. These opportunities laid the foundation for my academic success as well as my personal development. I also am very grateful to my siblings Cory, Krystin and Jesse for their continued love, friendship, and support.

I am also very grateful to my girlfriend Christina Malecki for all of her support and patience. She makes me a better person and has helped me to persist through graduate school. She has made me infinitely happy over the past several years, and I wish to express my gratitude and love toward her for her prayers and everything she has done for me. I would also like to thank her parents, Fran and Jerry Malecki, for all of their support and encouragement.

Finally, I would like to thank God for all of his blessings and his grace. I thank Him for all of the opportunities, experiences, and people He has brought into my life, and I thank him for answered prayers and for opened doors.

# TABLE OF CONTENTS

# LIST OF TABLES

## CHAPTER 4:

# LIST OF FIGURES

## CHAPTER 1:

## CHAPTER 2:

## CHAPTER 4:

Figure 1: The proposed reaction mechanism for the Berthelot reaction consists of three steps: (i) ammonia reacts with hypochlorite to form monochloramine at basic pH, (ii) monochloramine reacts with a phenol to form benzoquinone chlorimine, (iii) benzoquinone chlorimine reacts with a second phenol to form an indophenol. (iv) Sodium nitroferricyanide (III) dihydrate is a coupling reagent which increases the kinetics of step (ii).

Figure 2: The formation of indophenol cross-links results in an increase in the elastic restoring force of the hydrogel, which actuates an osmotic pressure, forcing water out of the hydrogel and thereby decreasing the volume of the gel. As a result, the spacing between diffracting planes in the PCCA decreases, and the wavelength of diffracted light blue-shifts proportional to $NH_3$ concentration.

Figure 3: After UV polymerization and functionalization, the photonic crystal ammonia sensor contains pendant 3-aminophenols which can be cross-linked via the Berthelot reaction mechanism in the presence of ammonia and hypochlorite.

Figure 4: Diffraction spectra of PCCA in presence of 300 μM $NH_3$. The PCCA blue-shifts continuously over the course of 120 min as $NH_3$ reacts with $OCl^-$ and 3-AMP to form an indophenol species which cross-links the hydrogel.

Figure 5: Diffraction blue-shift versus time for ammonia-sensing PCCA in BBS at pH 9.2 containing 600 μM $OCl^-$. The sensor displays distinctly different rates of diffraction shift for differing $NH_3$ concentrations; the control, containing no $NH_3$, actually red-shifts. The error bars are the average over the different time measurements of the standard deviation between replicate trials ($\lambda_{diffraction} = \pm 1.46$ nm, N = 3). The relative standard deviation remained fairly constant over time.

Figure 6: Calibration curve based on the response of our sensor to $NH_3$ in BBS (pH=9.2) containing 600 μM $OCl^-$ at 60 and 120 min. This sensor shows a linear response between 30 and 150 μM $NH_3$ at 60 min.

Figure 7: We measured the PCCA response of four spiked serum samples and an un-spiked sample. All samples contained 600 μM $OCl^-$ and had a pH of 9. We found the serum contains $NH_3$ on the order of the physiological concentration for healthy adults. The error bars are the average of the standard deviation between replicate trials ($\lambda_{diffraction} = \pm 0.57$ nm, N = 3).

Figure 8: Calibration curve for the response of our sensor to $NH_3$ in a 1:1 solution of serum and BBS at 60 min. Concentrations of $NH_3$ were determined using the Vitros Autoanalyzer. Error bars are equal to the standard deviation ($\lambda_{diffraction} = \pm 0.57$ nm, N = 3).

**CHAPTER 5:**

Figure 1: a) displays the spectral response as a function of time for three different OP solutions which contain OP levels below stoichiometry with the AChE attached to the sensor. The number of OP moles present increases from black to green to red. The amount of OP can be quantified according to the final equilibrium spectral shift of the sensor. b) displays the spectral response of the sensor to OP concentrations which are above stoichiometry with the AChE. The amount of OP present increases from blue to black. If the sensing volume is held constant, a solution containing more OP will saturate the diffraction faster. By selecting a point in time, $t$, which occurs prior to saturation, the spectral shift can be correlated to the amount of OP in the solution.

# CHAPTER 1: INTRODUCTION

## 1.1 Background

In the past two decades, colloid science has become a prominent area of nanotechnology research, primarily in the development of novel photonic crystal materials for non-linear optics, switching and sensing applications. The Asher Research Group at the University of Pittsburgh has been at the forefront of this expanding nanotechnology frontier, and has demonstrated significant novel contributions to the field by introducing the polymerized crystalline colloidal array (PCCA) technology, which combines the distinct optical properties of colloidal crystals coupled with the sensitivity of polymer hydrogels to their environment, resulting in a robust photonic crystal material which can be utilized for diverse applications.[1-20] These PCCA materials take advantage of the unique optical properties of periodic nanomaterials. The array of particles cause a modulation of the medium dielectric constant, resulting in optical diffraction pehenomena which give rise to distinct and narrow diffraction bands. The diffraction of PCCAs can be used for chemical sensing and optical switching applications. These materials can be functionalized with chemical recognition elements to take advantage of the extreme sensitivity of polymers to their chemical environments, resulting in sensors which can specifically recognize small molecules, single ions, and large molecules such as proteins.

## 1.2 Colloidal Self-Assembly and Bragg Diffraction

Colloidal particles which are highly charged and sufficiently monodisperse will self-assemble into a periodic three-dimensional lattice, like that of a crystal, forming a

crystalline colloidal array (CCA, Fig. 1).[4,5,7,15,21,22] CCAs form in low ionic strength

aqueous media due to the electrostatic repulsion of the thousands of highly charged

sulfonate and carboxylate groups that are present on the surface of colloidal particles.

These arrays are non-closed packed structures which have spacings between the particles

that are several times the diameter of the colloidal particles themselves. The arrays for

100-150 nm polystyrene particles can be either face-centered cubic (fcc) or body-

centered cubic (bcc) in structure, depending on the volume fraction of colloid present in

solution. BCC crystals typically arise when the volume percentage of colloidal particles

is less than 6%, while FCC crystals typically arise for volume fractions greater than 6%

(Fig. 1).[5] The lattice spacings are typically much greater than the particle diameters due

to interspherical repulsion between the particles which occurs over large distances. The

electric potential U(r) of a charged particle's surface, defined by Equation (1), is

dependent upon the sphere radius (a), the medium dielectric constant ($\varepsilon$), the interparticle

distance (r), the charge (Z), and the Debye-Hückel parameter ($\kappa$):[23]

$$U(r) = \frac{Z^2 e^2}{\varepsilon} \left[ \frac{e^{\kappa a}}{1 + \kappa a} \right]^2 \frac{e^{-\kappa r}}{r} \tag{1}$$

The Debye-Hückel parameter ($\kappa$) is essentially a measure of the length over which

two charged particles can electrostatically interact, and is defined by Equation (2), where

$k_B$ is the Boltzmann constant, $\varepsilon$ is the medium dielectric constant, $n_p$ is the number of

dissociated ions, Z is the charge of the ions, and $n_i$ is the concentration of ionic

impurities.[23-25]

$$\kappa = \sqrt{\frac{4\pi e^2}{\varepsilon k_B T} (n_p Z + n_i)} \tag{2}$$

The distance $1/\kappa$ is defined as the Debye length, which is the length at which the potential U(r) drops to 1/e of its value (Fig.2). The Debye length defines the radius of the electrical double layer surrounding the colloidal particle. For ~ 100-150 nm polystyrene colloidal particles typically used by the Asher group, this distance is about 700 nm.[1-20] The Debye length decreases as the concentration of ionic impurities in the solution increases (Fig. 2).

a)                                         b)
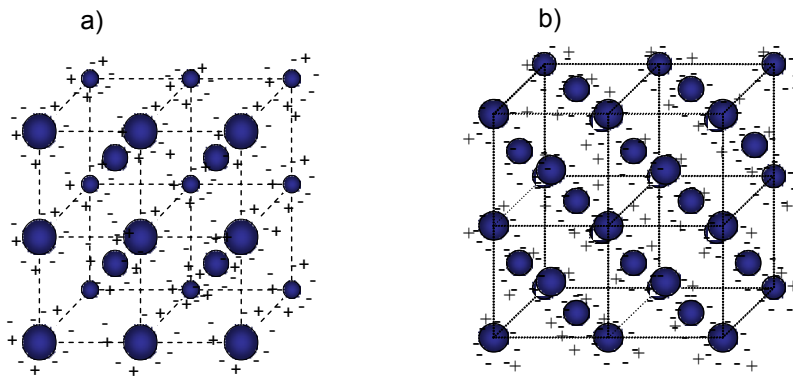


**Figure 1: Highly-charged monodisperse colloidal particles form crystalline lattices in low-ionic strength media. a) shows a body-centered cubic (BCC) array, while b) shows a face-centered cubic (FCC) array.**
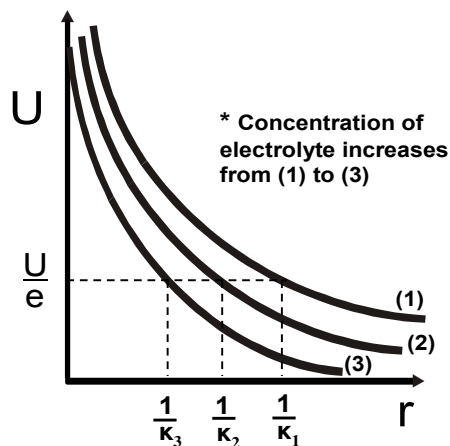


**Figure 2: The potential of the charged colloidal particle falls off with distance, and at $1/\kappa$ the double layer is 1/e of its original value. Increasing ionic strength causes the double layer thickness to decrease.**

highly-charged colloidal particles self-assemble in low-ionic strength media to form a crystalline colloidal array. These CCAs will diffract light in the UV, visible, and IR regions in a similar manner to the way atomic crystals diffract x-rays.[1-20] Numerous layers of crystal lattice planes exist within these colloidal arrays, called Bragg planes. These planes reflect all light which meets the Bragg condition coherently, resulting in constructive interference of the scattered light. Bragg's law is as follows:

$$m\lambda = 2nd \sin \theta \qquad (3)$$

where $m$ is the order of diffraction, $\lambda$ is the wavelength of light diffracted, $n$ is the refractive index of the medium, $d$ is the spacing between diffracting planes in the crystal lattice, and $\theta$ is the Bragg glancing angle. Different diffracting crystal planes have different lattice spacings, consequently they Bragg diffract varying wavelengths of light. Light diffracted from the 111 diffraction plane of the crystal is most intense because $\sin \theta$ is unity. CCAs diffract very narrow wavelengths of light, and the lattice spacing of the crystal can be tuned such that the crystal will Bragg diffract light in the visible region of the spectrum. The Asher group utilizes CCAs for the purposes of fabricating hydrogel sensing materials with embedded colloidal arrays tuned to visible diffraction wavelengths. Changes in the hydrogel volume result in either a decrease or increase of the spacing between diffracting planes of the embedded CCA, which causes corresponding changes in the wavelength of light Bragg diffracted from the 111 crystal plane.
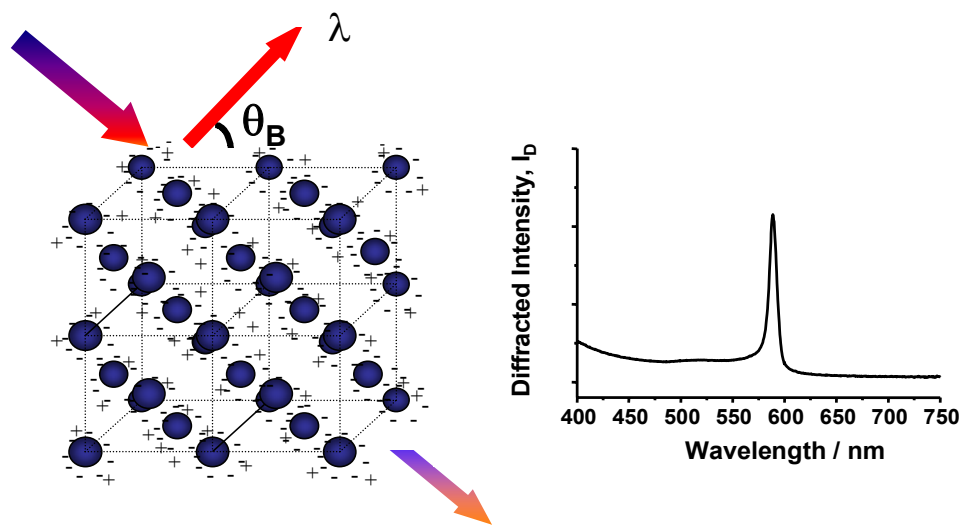
**Figure 3:** Light that is incident on the system passes through a CCA, except for a narrow range of wavelengths of light which meet the Bragg condition. These wavelength are diffracted by the crystal, resulting in a distinct diffraction peak when examined with a fiberoptic spectrometer (right). The CCA also displays a distinct color corresponding to the wavelength diffracted when examined with the naked eye. Figure courtesy of Dr. Chad E. Reese.

## 1.3   Colloidal Particle Synthesis

Polystyrene colloidal particles between 100 and 300 nm in diameter can be made using an emulsion polymerization technique. Typically, the chemical ingredients for an emulsion polymerization include: water as the polymerization medium, a water-soluble free-radical initiator, an emulsifier, and a monomer which is only slightly water-soluble.

To make 120 nm polystyrene spheres, a standard emulsion polymerization protocol is utilized.[21, 26] The roundbottom reaction vessel (Kontes) is hooked to an oil bath (VWR Scientific Products) in order to maintain the solution temperature during the reaction. 137 ml of nanopure $H_2O$ and 0.172 g of $NaHCO_3$ buffer (Fisher) are mixed in the flask and purged with nitrogen for approximately 30 minutes. 2.0 g of MA-80

surfactant (Cytec) are added in three 5 ml washings. After 10 minutes, the nitrogen purge is removed, and the surface of the solution is blanketed with nitrogen. Styrene (Aldrich), the monomer, and divinylbenzene (DVB, Aldrich), the cross-linker, are mixed in an addition funnel and purged with nitrogen for 20 minutes. The reaction vessel is then heated to $50^{o}C$ and stirred at 125 RPM. Once the solution reaches $50^{o}C$, the stirring is increased to 350 RPM, and the monomer/cross-linker mixture is introduced to the solution at a constant rate. Then, 2.9 g of COPS-1 (Rhone-Poulenc), an ionic comonomer, is then added in one 5 ml addition. The COPS-1 serves to increase the surface charge on the particle. Upon addition of COPS-1, the reaction is heated to $70^{o}C$. Once the temperature equilibrates, 0.75 g of the initiator, sodium persulfate ($N_2H_8S_2O_8$, Aldrich) is dissolved in 5 ml nanopure water and added to the mixture. The system is then refluxed for 3 hours. After reflux, the solution is cooled to room temperature and filtered through glass wool to remove clumps. The colloid is then dialyzed to clean it up using 2,000,000 MWCO PVDF dialysis tubing (Spectrum Laboratories) for two weeks. The dialysis water is changed daily until the conductivity measurements of the dialysis water are the same as those of nanopure water, which indicates that all of the ionic contaminants have been removed from the system. AG 501-X8 (D) mixed bed ion exchange resin (Bio-Rad) is then added to the colloidal solution during storage to remove further ionic impurities. See Appendix for all particle synthesis-related chemical structures.

Once cleaned, the colloidal particles display a very iridescent diffraction. The 111 plane of the array aligns itself against the walls of the container, so the diffraction can be easily recognized.
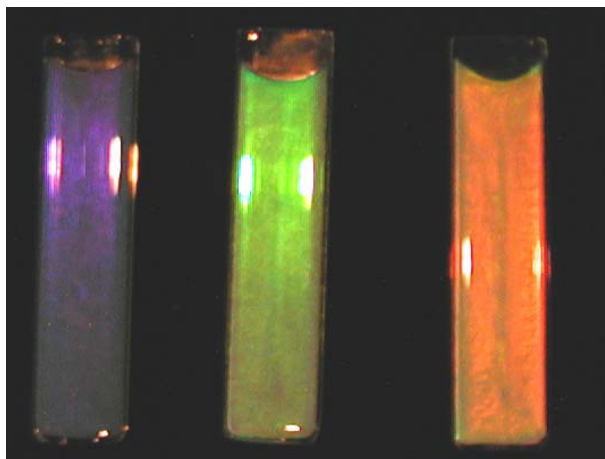
**Figure 4: CCAs display very iridescent diffraction after removal of ionic impurities. Above, the CCA diffraction red-shifts when diluted with H₂O because the spacing between diffracting crystal planes increases, allowing the particles to move farther apart to minimize their repulsive forces. Photograph courtesy of Dr. Anjal C. Sharma.**

Once the colloidal particles are made, several techniques can be used to analyze them. Particle size and polydispersity are measured using a Zeta-Plus Particle Sizer (Brookhaven Instruments Corporation). The effective diameters of the colloidal particles used in the Asher lab for sensing applications are typically in the 100-150 nm range, with typical polydispersities <5%. Monodisperse particles will have a more ordered lattice than polydisperse particles due to the uniformity of the charge. The resultant Bragg diffraction peak will be narrower or "sharper" for more ordered lattices due to the fact that there are fewer interfering planes present. The charge density can also be determined by performing conductimetric titration of the samples.

## 1.4 Flory Polymer Theory

CCAs give rise to interesting phenomena, but in their pure liquid form ionic impurities can "melt" the CCA lattice by screening the repulsion between the double layers of particles. This screening causes disorder in the system and loss of the particles' periodicity.[27,28] CCA disordering can be prevented by polymerizing it into a hydrogel network.[29-31] The lattice ordering of a CCA embedded in a hydrogel is preserved and becomes much less susceptible to disordering by high ionic strength solutions.

Before we discuss fabrication of hydrogels containing CCA (Polymerized Crystalline Colloidal Arrays, PCCAs), we must discuss the utility of immobilizing the array in a hydrogel network. Hydrogels are polymer networks filled with liquid media. The hydrogel volume phase transition can be elicited via three mechanisms, as outlined by Flory-Huggins theory.[32] The total Gibbs free energy of the hydrogel system is a sum of three individual free energies:

$$\Delta G_{tot} = \Delta G_{ion} + \Delta G_{elas} + \Delta G_{mix} \tag{3}$$

where the three contributing free energies are the ionic free energy ($\Delta G_{ion}$), the free energy of the elasticity of the hydrogel ($\Delta G_{elas}$, based upon cross-linker concentration), and the free energy of mixing ($\Delta G_{mix}$) of the hydrogel. These free energies, when divided by the volume change of the polymer, each contribute to the overall osmotic pressure, $\Pi_{tot}$, of the system according to the same fashion:

$$\pi_{tot} = \pi_{ion} + \pi_{elas} + \pi_{mix} \tag{4}$$

Thus, changes in any of these parameters actuate changes in the osmotic pressure of the hydrogel and cause the hydrogel to shrink or swell accordingly. The ability to polymerize CCAs into hydrogels allows for the fabrication of sensors which can utilize the contributions of each of these free energy parameters to produce volume transitions which result in visible changes in diffraction as the hydrogel responds to an analyte.

## 1.4.1 Ionic Free Energy

The ionic electrostatic forces operate in the following manner. If the analyte creates a charged species upon binding to the hydrogel backbone, then there exists a local concentration inside the hydrogel of ionic charges which is greater in concentration than the ionic charge in the solution outside the hydrogel.[32] Thus, an electrochemical gradient called a Donnan potential exists. The Donnan potential results in an osmotic potential between the interior and exterior of the gel, and as a result water containing counterions rushes in and causes the gel to swell. The degree of swelling is proportional to the number of bound charges.[33] The Donnan potential, however, is attenuated as the ionic strength of the solution increases, and at concentrations of salt greater than 10 mM, the Donnan potential is completely swamped out.[33] Thus, the ionic response of hydrogels is only useful for sensing applications in low ionic strength solutions.

**1.4.2 Free Energy of Elasticity**

The second type of free energy dependence of hydrogel swelling is the free energy of elasticity. This is based primarily upon the cross-link density of the hydrogel.[32] Sensors have been made which contain molecular recognition agents which bind analytes at two or more locations, resulting in the formation of new cross-links in the hydrogel matrix. This serves to increase the elastic restoring force of the hydrogel, which causes it to contract and blue-shifts the wavelength of light diffracted. In some cases, the analyte can also be washed out, breaking the cross-link and causing the sensor to swell, red-shifting the diffraction.

**1.4.3 Free Energy of Mixing**

The final free energy contribution to hydrogel volume comes from the free energy of mixing, which is a measure of the degree of solvation of the hydrogel in the presence of the solvent.[32] The degree of solubility is measured by the Flory-Huggins interaction parameter $\chi$.[32] This parameter can be experimentally determined, and is essentially a measure of the solubility of the hydrogel. The type of solvent also contributes to the solubility of the hydrogel. Also, the attachment of an analyte, or changes in conformation of bound groups, can cause changes in the solubility of the hydrogel. Larger $\chi$ parameter values mean that the hydrogel is less soluble, so it will shrink in the solvent and display a more blue-shifted diffraction than a hydrogel with a smaller $\chi$ parameter. A

polyacrylamide hydrogel, for example, will have a lower χ parameter (be more swollen) in water than in an acetone solvent.

## 1.5 PCCA Preparation

The Asher research group has developed several methods for polymerizing CCAs within hydrogel networks, which creates a stable environment that preserves the lattice ordering of the embedded CCA and which also takes advantage of the rich volume transitions that hydrogels undergo in response to aqueous environment..[29-31] The rich volume phase transitions undergone by hydrogels in response to their aqueous environments are well-characterized.[30,32, 34-38] The hydrogel network with an embedded colloidal array is called a Polymerized CCA (PCCA).

A typical recipe for making a photopolymerized PCCA follows. Total volume is kept ~ 2 ml. Acrylamide (0.10 g, 1.4 mmol, Fluka), N,N'-methylenebisacrylamide (2.5 mg, 16.2 μmol, Fluka), colloid suspension (2.0 g, 5-10% w/w dispersion, polystyrene latex spheres, ~110 nm diameter[18-21, 26] in Nanopure water, AG501-X8 (D) ion exchange resin (~0.1 g, 20-50 mesh, mixed bed, Bio-Rad), and 10% DEAP (7.7 μL, 3.84 μmol; Diethoxyacetophenone; Aldrich) in DMSO (Fisher) are mixed in a 2-dram vial. Two quartz discs (Esco Products, Inc.) are clamped together with a 125 μm parafilm spacer (Pechiney Plastic) between them. The mixture is injected into the cavity between the quartz discs, and they are placed under a mercury arc lamp (Blak-Ray Model B-100A),

which has a filter that allows only transmission of 366 nm UV light. The mixture is left to polymerize under UV light for 2 hours. After two hours, the quartz cell is separated in nanopure water, and the PCCA is allowed to equilibrate. Figure 5 displays photographs of the CCA before polymerization and PCCA after polymerization.
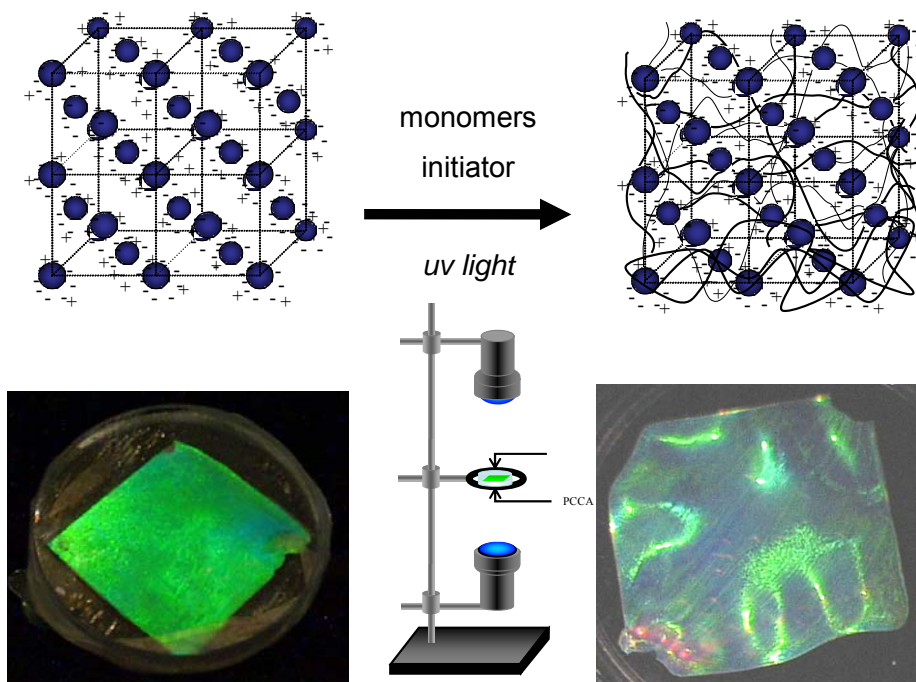


**Figure 5: CCA are mixed with monomers, cross-linkers, and a non-ionic photoinitiator and subjected to 365 nm UV light for 2 hrs (bottom middle). The system is initially entirely liquid (bottom left). After polymerization, the quartz cell is opened in water, and the CCA embedded in the polymer hydrogel maintains its iridescent diffraction. Photographs of CCA, PCCA courtesy of Dr. Chad E. Reese.**

Once the PCCA has been polymerized, opened, and rinsed to remove excess monomer, the polymer backbone can be functionalized utilizing a vast assortment of chemistries to attach molecular recognition agents for specific analytes. These recognition agents can be macrocycles for ion recognition, small molecules for covalent binding of other small molecules, pH-sensitive moieties, or large proteins such as antibodies or enzymes. The addition of a molecular recognition agent to the backbone

transforms the PCCA into an Intelligent PCCA (IPCCA). The IPCCA is capable of recognizing a specific analyte. The binding of the analyte elicits a volume change in the hydrogel; a change in the volume of the hydrogel causes a consequent change in the spacing between diffracting planes of the embedded CCA, and results in a shift of the wavelength of diffracted light proportional to the analyte concentration.

## 1.6 Overview of Research Program

The work reported herein discusses the development of three separate photonic crystal hydrogel sensors, each of which exploits a different free energy of mixing parameter to elicit sensing responses from the IPCCA hydrogel materials.

Chapter 2 describes a polymerized crystalline colloidal array (PCCA) photonic crystal sensing material which senses the organophosphorus compound parathion at ultra-trace concentrations in aqueous solutions. A periodic array of colloidal particles is embedded in a hydrogel network with a lattice spacing such that it Bragg diffracts visible light. The molecular recognition agent for the sensor is the enzyme acetylcholinesterase (AChE), which binds organophosphorus compounds irreversibly, creating an anionic phosphonyl species. This charged species creates a Donnan potential, which swells the hydrogel network, which increases the embedded particle array lattice spacing and causes a red-shift in the wavelength of light diffracted. The magnitude of the diffraction red-shift is proportional to the amount of bound parathion. The AChE-PCCA acts as a dosimeter for parathion since it irreversibly binds the organophosphate. Parathion concentrations as low as 4.26 fM are easily detected.

In Chapter 3, we describe the development of an intelligent polymerized crystalline colloidal array (IPCCA) photonic crystal sensing material which reversibly senses the organophosphate compound methyl-paraoxon at micromolar concentrations in aqueous solutions. The sensor operates via changes in the free energy of mixing of the hydrogel. A periodic array of colloidal particles is embedded in a poly-2-hydroxyethylacrylate hydrogel. The particle lattice spacing is such that the array Bragg diffracts visible light. We utilize a bimodular sensing approach in which the enzyme organophosphorus hydrolase (OPH) catalyzes the hydrolysis of methyl-paraoxon at basic pH, producing p-nitrophenolate, dimethylphosphate, and two protons. The protons decrease the pH and create a steady-state pH gradient. Protonation of the phenolates attached to the hydrogel makes the free energy of mixing of the hydrogel less favorable, which causes the hydrogel to shrink. The IPCCA's lattice constant decreases, which blue-shifts the light diffracted. The magnitude of the steady-state diffraction blue-shift is proportional to the concentration of methyl-paraoxon. The current detection limit is 0.2 µM methyl-paraoxon.

Chapter 4 describes an ammonia sensitive material by coupling the Berthelot reaction to our Polymerized Crystalline Colloidal Array (PCCA) technology. This sensor operates through changes in the elasticity of the hydrogel, the third free energy parameter, which arise due to creation of cross-links. The material consists of a periodic array of highly charged colloidal particles embedded in a poly-hydroxyethylacrylate hydrogel. In the Berthelot reaction, ammonia, hypochlorite, and phenol react to produce

14

the dye molecule indophenol blue in an aqueous solution. We utilize this reaction in our sensor by covalently attaching 3-aminophenol to the hydrogel backbone, which forms cross-links through the Berthelot mechanism. Ammonia reacts with hypochlorite, forming monochloramine, which then reacts with a pendant aminophenol to form a benzoquinone chlorimine. The benzoquinone chlorimine reacts with another pendant aminophenol to form a cross-link. The creation of new cross-links causes the hydrogel to shrink, which decreases the lattice spacing of the embedded colloidal array. This volume change results in a blue-shift in the diffracted light proportional to the concentration of $NH_3$ in the sample. The reaction is irreversible. We demonstrate that the $NH_3$ photonic crystal sensing material is capable of quantitative determination of ammonia concentrations in the physiological range (50 – 350 $\mu M$ $NH_3$) in human blood serum.

Chapter 5 summarizes the work and suggests future direction for each of the projects, including optimization and application. Chapter 5 also discusses the novelty of these photonic crystal sensing materials and underscores the importance of these colloidal particles and PCCAs with respect to their utility as materials for optics and coatings as well as their analytical utility as sensors for a diverse assortment of analytes.

## 1.7 References

(1)   Krieger, I. M., O'Neill, F. M., *J. Am. Chem. Soc*. **1968,** *90*, 3114.

(2)   Hiltner, P. A., Krieger, I. M., *J. Phys. Chem.* **1969,** *73*, 2386.

(3)   Hiltner, P. A., Papir, Y. S., Krieger, I. M., *J. Phys. Chem*. **1971,** *75*, 1881.

(4)   Carlson, R. J., Asher, S. A., *Appl. Spec*. **1984,** *38*, 297.

(5)     Rundquist, P. A., Photinos, P., Jagannathan, S., Asher, S. A., *J. Chem. Phys.*, **1989,** *91*, 4932.

(6)     Asher, S. A., Holtz, J. H., Liu, L., Wu, Z., *J. Am. Chem. Soc*. **1994,** *116*, 4997.

(7)     Weissman, J. M., Sunkara, H. B., Tse, A. S., Asher, S.A., *Science* **1996,** *274*, 959.

(8)     Pan, G., Sood, A. K., Asher, S.A*., J. Appl. Phys.* **1998,** *84*, 83.

(9)     Pan, G., Tse, A. S., Kesavamoorthy, R., Asher, S. A., *J. Am. Chem. Soc*. **1998,** *120*, 6518.

(10)  Ito, K., Nakamura, H., Ise, N., *J. Chem. Phys*. **1986,** *85*, 6136.

(11)  Liu, L., Li, P., Asher, S. A., *J. Am. Chem. Soc*. **1997,** *119*, 2729.

(12)  Monovoukas, Y., Gast, A. P., *J. Colloid Interface Sci*. **1989,** 128, 533.

(13)  Kesavamoorthy, R., Rajalakshmi, M., Babu R.C., *J. Phys. Condens. Matter* **1989,** *1*, 7149.

(14)  Okubo, T., *Acc. Chem. Res*. **1988,** *21*, 281.

(15)  Asher, S. A., Flaugh, P. L., Washinger, G., *Spectroscopy* **1986,** *1*, 26.

(16)  Asher, S.A., U.S. Patents 4,627,689 (**1986**)., 4,632,517 (**1986**), 5,281,370 (**1994**).

(17)  Carlson, R.J., Asher, S.A., *Appl. Spectrosc*. **1984,** *38*, 297.

(18)  Pan, G., Kesavamoorthy, R., Asher, S. A., *Phys. Rev. Letters*. **1997,** 78, 3860.

(19)  Pan, G., Kesavamoorthy, R., Asher, S. A., *J. Am. Chem. Soc*. **1998,** *120,* 6525.

(20) Asher, S. A., U.S. Patent 5,452,123 (**1995**).

(21) Reese, C.E., Guerrero, C.D., Weissman, J.M., Lee, K., Asher, S.A., *J. Colloid Interface Sci.* **2000**, *232*, 76-80.

(22) Flaugh, P.L., O'Donnell, S.E., Asher, S.A., *Appl. Spectrosc.* **1984**, *38*, 847-850.

(23) Atkins, P. *Concepts in Physical Chemistry*. **1995**, W.H. Freeman and Company, New York.

(24) http://www.dur.ac.uk/sharon.cooper/lectures/colloids/interfacesweb2.html

(25) Everett, D.H. *Basic Principles of Colloid Science.* **1988**, Royal Society of Chemistry, London, U.K.

(26) Reese, C.E. Ph.D. Thesis, **2003,** The University of Pittsburgh.

(27) Hachisu, S., Kobayashi, Y., Kose, A., *J. Col. Int. Sci*. **42**, 342 (1973).

(28) Dickinson, E., Parker, R., *Chem. Phys. Lett.* **79**, 578 (1981).

(29) Holtz, J. H., Asher, S. A., *Nature* **1997,** *389*, 829.

(30) Holtz, J. H., Holtz, J. S. W., Munro, C., Asher, S. A., *Anal. Chem.* **1998,** *70*, 780.

(31) Asher, S. A., Holtz, J., Weissman, J., Pan, G., *MRS Bulletin* **1998,** *23*, 44.

(32) Flory, P.J. *Principles of Polymer Chemistry*. **1953,** Cornell University Press; New York.

(33) Lee, K.; Asher, S.A. *J. Am. Chem. Soc.* **2000**, *122*, 9534-9537.

(34) Annaka, M.; Tanaka, T., *Nature*, **1992**, *355*, 430.

(35) Mafe, S.; Manzanares, J.A.; English, A.E.; Tanaka, T. *Phys. Rev. Lett.* **1997**, *79*, 3086.

(36)  English, A.E.; Tanaka, T.; Edelman, E.R.; *J. Chem. Phys.* **1984,** *107,* 1645.

(37)  Tanaka, T. *Sci. Am.* **1981**, *244*, 124.

(38)  Tanaka, T.; Niccolini, C., Ed. in *Structure and Dynamics of Biopolymers*,

Series E: Dordrecht, **1986**, pp. 237-257.

**CHAPTER 2:**

## Acetylcholinesterase-based Organophosphate Nerve Agent Sensing Photonic Crystal

## 2.1 Introduction

There is currently an urgent need for efficient, rapid detection of organophosphorus (OP) compounds. OP compounds are prominently used by the agricultural industry in the United States and worldwide in the form of pesticides and insecticides. These OPs have been detected in streams draining from urban watersheds and in agricultural watersheds.[1] OPs also occur in the form of chemical warfare nerve agents such as sarin, cyclosarin, VX, and tabun. These compounds are potent irreversible inhibitors of nervous system function,[2,3] and are thus quite toxic.

At present, there are several techniques available for determining the concentration of OPs in solution. GC-MS and HPLC techniques are commonly used,[4] and show detection limits in the nanomolar concentration range.[5] However, these techniques are time-consuming and require extensive sample preparation in order to detect environmentally significant levels of OPs. Field detection appears impractical.

There are also detection schemes which utilize flow-injection methods in which acetylcholinesterase (AChE) is immobilized inside or upon a polymer. In these methods the AChE is exposed to the OP, then a solution is added containing a substrate and a

reagent which reacts to form a chromophore. The chromophore absorbance determines the enzyme activity, which is decreased by binding of the OP. Leon-Gonzales et.al.[6] achieved 8 nM detection limits for OPs using this technique.

Molecularly imprinted polymer (MIP) sol-gel films with high selectivity toward specific OP species are also used.[7] These MIPs utilize functionalized silanes as templates to selectively bind OPs. This OP binding has been coupled to fluorescence and electrochemical techniques to determine the OP concentration.

Leblanc et. al.[8] have used layer by layer (LbL) deposition technique to make Langmuir-Blodgett multilayers of the enzymes acetylcholinesterase, organophosphorus hydrolase (OPH)[9,10] and organophosphorus acid anhydrolase (OPAA)[10]. They achieved nM detection limits of the pesticide paraoxon[10,11] by monitoring fluorescence.

Amperometric detectors which sense OPs at nM levels have also been fabricated. These detectors utilize AChE [12], or organophosphorus hydrolase[13,14] immobilized upon electrodes. Mulchandani et.al. [13] achieved detection limits of 70 nM OP, while Sacks et al.[14] detected nM concentrations of parathion. These techniques appear practical for field detection because the sensors are easily miniaturized and require compact, inexpensive instrumentation and require only modest sample preparation. However, these techniques may suffer interference from other oxidizable substances which may be present in real (field) samples. [14]

In the work here we utilize AChE as the molecular recognition agent for parathion, an OP. AChE is an enzyme which functions at the neural synapse to hydrolyze the neurotransmitter acetylcholine to acetate and choline.[15] The hydrolysis depolarizes the nerve so that it can undergo another conduction event.

OPs inhibit AChE by irreversibly blocking substrate turnover. The OP binds to the active site serine, producing a phosphonyl-enzyme complex. When AChE is phosphorylated, it cannot function and the nerve remains polarized.[15] Fig. 1 depicts the phosphorylation of AChE by parathion and its subsequent reactions. An anionic tetrahedral intermediate forms, [16,17] which dealkylates to form the "aged" product, which is a stable anionic phosphonyl adduct.[18] Millard et al. demonstrated using X-ray crystallography that the aged form of the phosphorylated enzyme involves a stable anionic adduct. [19]
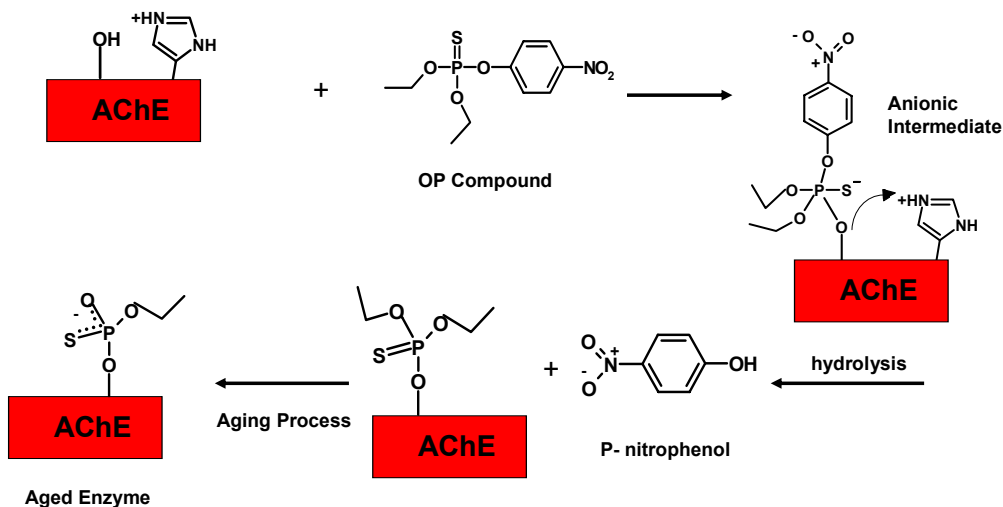


**Figure 1: Phosphorylation of AChE by parathion results in a charged intermediate form, which in aging undergoes dealkylation to form a stable anionic phosphonyl adduct, which irreversibly inhibits AChE.**

Our OP sensor is based on our polymerized crystalline colloidal array (PCCA) photonic crystal sensing technology. These PCCAs utilize an array of colloidal particles[20-25] polymerized into an acrylamide hydrogel[26-29] which Bragg diffracts light in the visible spectral region (Fig. 2). The molecular recognition group, AChE, is covalently attached to the hydrogel to bind the analyte of interest and to actuate a volume increase proportional to the concentration of analyte. The hydrogel volume increase redshifts the wavelength of light diffracted. Thus, shifts in the wavelength of diffracted light are proportional to the analyte concentration. Our AChE PCCA sensor relies upon a volume phase transition of the hydrogel due to changes in the ionic free energy of the system.
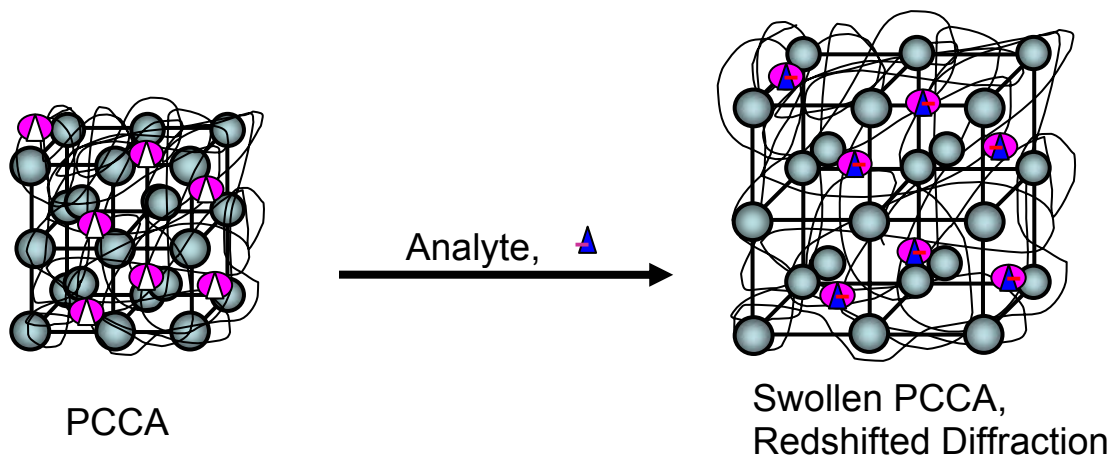


**Figure 2: A crystalline Colloidal Array (CCA) forms in an fcc structure due to electrostatic repulsion between particles. The particle spacings are set such that they diffract visible light. Polymerized CCA (PCCA) are formed by polymerization of an acrylamide hydrogel network around the CCA. The PCCA backbone is functionalized with a molecular recognition agent, which binds the analyte, actuating either a shrinkage or a swelling of the hydrogel network. The embedded CCA lattice spacing changes as the volume changes, shifting the diffracted wavelength and the perceived color of the PCCA.**

The wavelength of light ($\lambda_o$) diffracted follows Bragg's Law: $\lambda_o = 2\,n\,d\,\sin\theta$. In our AChE-PCCA light is diffracted by the fcc 111 plane of the embedded array of particles. $\lambda_o$ depends upon the plane spacing, d, the refractive index of the system, n and the incident angle of the light, $\theta$, which is the Bragg glancing angle. $\sin\theta$ is unity since we are sampling back-diffraction of light normally incident to the 111 plane.

## 2.2 Experimental

### 2.2.1 PCCA Preparation

Fig. 3 depicts the synthesis and functionalization of the PCCA. Acrylamide (0.10 g, 1.4 mmol, Fluka), N,N'-methylenebisacrylamide (2.5 mg, 16.2 μmol, Fluka), a colloid suspension (2.0 g, 5-10% w/w dispersion, polystyrene latex spheres, 110 nm diameter[20-25]) in Nanopure water (Barnstead), AG501-X8 (D) ion exchange resin (~0.1 g, 20-50 mesh, mixed bed, Bio-Rad) and 10% DEAP (7.7 μL, 3.84 μmol; Diethoxyacetophenone; Aldrich) in DMSO (Fisher) were mixed in a 2-dram vial. The mixture, which was centrifuged to remove the ion exchange resin, was injected between two quartz disks separated by a 125 μm-thick Parafilm spacer. The colloidal particles self-assemble into a CCA, giving rise to a liquid film which diffracts light. The film was exposed to 365 nm UV light from mercury lamps (Blak Ray) for 2 hours. A polyacrylamide hydrogel network forms around the CCA, resulting in a Polymerized CCA (PCCA)[26-29]. The cell

enclosing the PCCA was then opened in Nanopure water and the PCCA film allowed to equilibrate.

**2.2.2 Chemical Modification of Hydrogel Backbone**

The PCCA was transferred from 100% $H_2O$ to 100% DMSO in 25% increments over the course of 1 hour. The PCCA was then placed into 200 mL of 10% (v/v) solution of ethylenediamine (Fisher) in DMSO. This solution was heated to $90^o$ C in a closed 500 mL roundbottom jacketed reaction vessel (Kontes). The reaction was allowed to proceed for 16 hrs. to convert the pendant amide groups to amines.[30] The PCCA was then removed and transferred stepwise back from DMSO to pure $H_2O$. After 2 hours of washing in Nanopure water the PCCA displayed a 574 nm diffraction maximum.
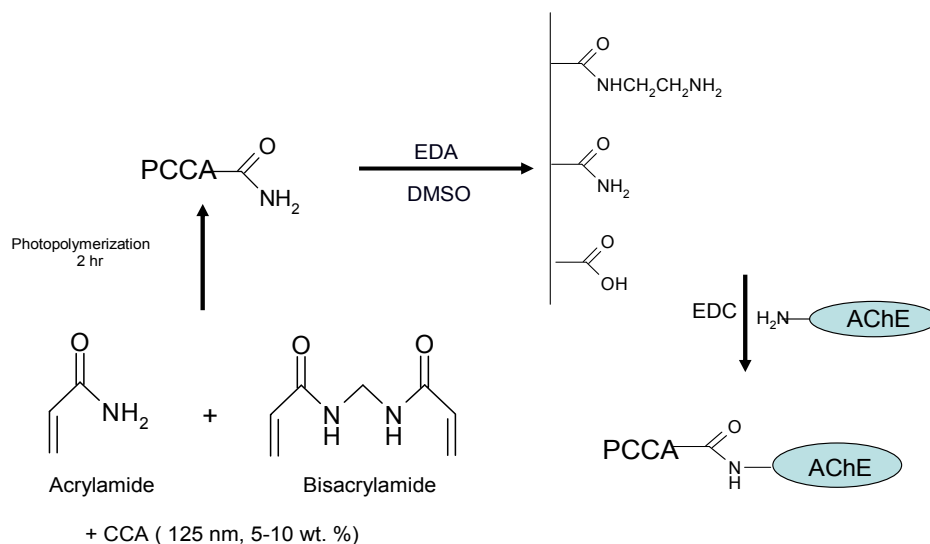


**Figure 3: Preparation and functionalization of AChE-PCCA hydrogel backbone.**

24

### 2.2.3 Attachment of Acetylcholinesterase to PCCA

A coupling solution of acetylcholinesterase (AChE; EC 3.1.1.7:V-S from electric

eel, MW 260 kDa, 806 units/mg solid, Sigma) was prepared by diluting 1.6 mg (2000

units) to a volume of 4 mL with 150 mM Tris buffer (Pierce Biotechnology) at pH 7.4.

The PCCA was pre-incubated in the AChE solution for 48 hours. The PCCA was

removed from the AChE solution and dipped into a solution of 1-ethyl-3-(3-

dimethylaminopropyl) carbodiimide hydrochloride (EDC; 0.032 g, 167 μmol, Pierce) in 2

mL of 150 mM Tris buffer (pH 7.4). The PCCA was then placed back in the AChE

solution. Coupling was then allowed to proceed for 2 hours, after which the PCCA was

incubated for 48 hours in 150 mM Tris to exchange out uncomplexed AChE.

The initial PCCA diffraction of 574 nm redshifts to 636 nm due to attachment of AChE,

presumably due to an increased free energy of mixing; AChE attachment results in an

increased hydrogel hydrophilicity.

### 2.2.4 Functionality Test of AChE-PCCA

The sensor was tested for enzyme activity with acetylthiocholine iodide (ATChI,

Sigma), a mimic of the natural substrate acetylcholine, using Ellman's acetylthiocholine

hydrolysis assay.[31] ATChI was added to 100 mL of 10 μM 5,5'-dithiobis(2-nitrobenzoic

acid) (DTNB; Sigma) dissolved in 150 mM Tris Buffer (pH 8.0). ATChI concentrations

were varied from 1 mM to 6 mM. The AChE-PCCA was then placed into the solution,

and the UV-Vis absorbance of the reaction solution was monitored against a 150 mM

Tris buffer background. Absorbance at 412 nm was recorded over a 5 minute time period

at selected time intervals. The hydrolysis of ATChI in the absence of enzyme was also monitored.

**2.2.5 Diffraction Measurements**

The diffraction of the PCCA was monitored using a fiber optic diode spectrometer with a tungsten halogen light source (Ocean Optics) using a reflectance probe. The high diffraction efficiency of the PCCA causes the light to be diffracted completely by the first 10-20 μm thickness of the PCCA[25].

The diffraction was measured in aqueous solutions containing the OP pesticide parathion (Chem Service, Inc.). Stock solutions were made by dissolving 9.8 μL of parathion (0.0124 g, 42.6 μmol) in 2 mL of methanol (Fisher), then diluting to 1 L with Nanopure water with vigorous stirring. A serial dilution was then done using Nanopure water. The parathion concentration ranged from 4.26 fM (4.26 x $10^{-15}$ M) to 42.6 μM (4.26 x $10^{-5}$ M). The pH was adjusted to ~ 7.0 using very small amounts of 0.1 M NaOH (Fisher). A buffer was not used in order to avoid attenuation of the Donnan potential by a high ionic strength. The AChE-PCCA was pre-equilibrated for 1 hour in Nanopure water (pH 7.0) to allow it to reach equilibrium volume before exposure to parathion solutions.

The AChE-PCCAs were exposed to 100 ml sample solutions at each parathion concentration, beginning with 4.26 fM parathion, until the diffraction peak stopped shifting, indicating that the system has reached saturation. Lower concentrations required approximately 30 min. to stabilize. Diffraction spectra were recorded, then the PCCA was rinsed with nanopure water for ½ hour. The post-rinsing diffraction wavelength was recorded at each concentration level tested. In a control measurement, an aminoethylated PCCA without AChE attached was exposed to a parathion solution to ensure that the diffraction response requires the presence of AChE.

We also performed control experiments which mimicked the parathion measurements by preparing solutions identical to those described above, but in the absence of parathion. AChE-PCCAs were exposed to these samples for half-hour intervals, followed by half-hour rinsing with Nanopure water, after which diffraction spectra were recorded.

Another control experiment used a series of very dilute parathion solutions which had previously been measured. An AChE-PCCA that had never sensed parathion was exposed to the solutions to test the hypothesis that the sensor acts dosimetrically, and that parathion was removed from solutions. In this case, the diffraction shift occurred only upon exposure to parathion solutions for which the previous sensor had saturated.

## 2.3 Results and Discussion

### 2.3.1 Determination of Bound Acetylcholinesterase

We monitored the aqueous solution hydrolysis of ATChI solutions exposed to an AChE-PCCA by using the Ellman's assay in order to quantify the amount of AChE attached to the PCCA before exposure to parathion. The AChE-PCCA displays Michaelis-Menten enzyme kinetics for the hydrolysis of ATChI. The linear rate of reaction was calculated for AChE over the first 5 min for each trial. The reaction rates (µmol ATChI/min) were then plotted against the substrate concentration to obtain a Michaelis-Menten plot (Fig. 4). From the plot, we calculate a maximum rate of ATChI hydrolysis of 2.4 µmol/min. One unit of enzyme is the amount required to hydrolyze substrate at a rate of 1 µmol/min, which indicates the presence of 2.4 units, or at least 3.9 x $10^{-12}$ mol of active AChE attached to the gel. This calculation would underestimate the amount of attached enzyme if its activity were decreased by the immobilization. The natural hydrolysis rate in the absence of enzyme was measured to be 30 nmol/min averaged over 30 minutes. It appears that AChE retains a significant portion of its activity upon attachment to the hydrogel, probably because the reactive site is located at the bottom of a 20 Å-deep gorge.[32]
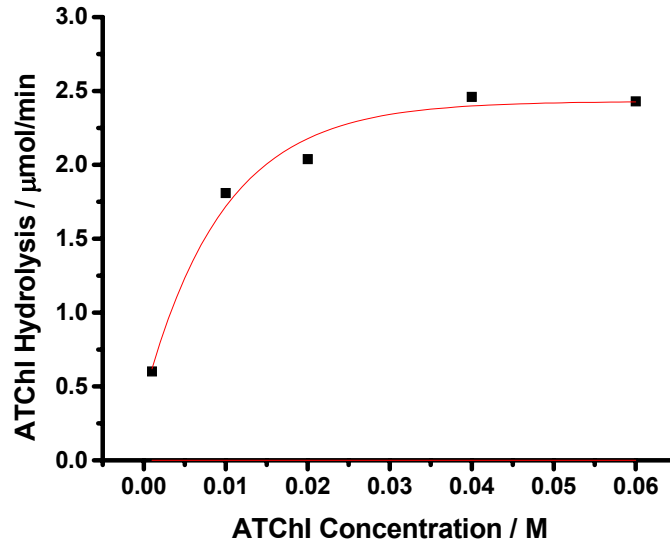
**Figure 4: Michaelis-Menten curve of Ellman's assay of AChE-PCCA confirms that some enzyme function is retained upon AChE attachment to PCCA backbone. The curve indicates that 2.4 units of active AChE are attached to the hydrogel backbone of the PCCA.**

**2.3.2 Response of AChE-PCCA to Parathion in Water**

Figure 5 shows the diffraction response of an AChE-PCCA upon exposure to 100 mL solutions of parathion of different concentrations. The sensor displays a 37 nm diffraction shift after only 15 min in the presence of 100 ml 4.2 fM parathion. Subsequent cycles of rinsing in Nanopure water and exposure to 100 ml solutions of increasing parathion concentrations yielded additional diffraction shifts until the diffraction response saturated (for a parathion concentration of ~42 pM) yielding a total spectral shift of ~120 nm.

For an infinite, irreversible binding constant, the amount of parathion that saturates our sensor would equal the number of moles of AChE attached to the PCCA.

29

We calculate that we require $4.3 \times 10^{-12}$ moles parathion for saturation, which is similar to the amount of AChE in the PCCA ($3.9 \times 10^{-12}$ moles). The parathion-induced redshift of the sensor is irreversible. Washing does not blue-shift the response.
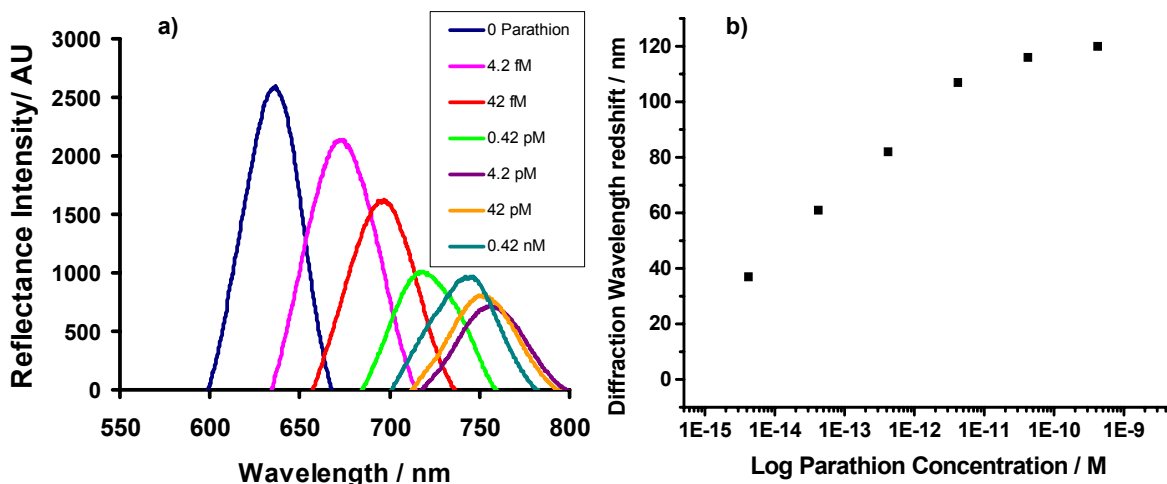


**Figure 5: a) Diffraction response of AChE-PCCA to 100 ml parathion solutions of varying concentrations. Saturation of response occurs at 42 pM parathion concentration. b) Diffraction red-shift versus log of parathion concentration. The AChE-PCCA displays saturation at 42 pM parathion solution exposure.**

In order to prove that parathion is complexed to the sensor, a series of subsaturation parathion solutions previously exposed to an AChE-PCCA sensor were exposed to a fresh AChE-PCCA. The hypothesis is that all of the parathion was removed by the first sensor. No significant change occurs in the diffraction wavelength of the second AChE-PCCA until the sensor is exposed to 42 pM parathion. At this concentration, the first AChE-PCCA saturated, thus, leaving some parathion in solution. Subsequent exposure of the second sensor to 0.42 nM and 4.2 nM parathion solutions completely saturates this second AChE-PCCA; all AChE sites become phosphorylated.

The lack of response by the second sensor to the first four depleted solutions proves that parathion was removed by the first AChE-PCCA.

### 2.3.3 Response Mechanism

Three control experiments were performed to confirm that the diffraction response was due to the anionic species formed when the parathion inhibits the AChE. An aminoethylated, AChE-free PCCA was exposed to parathion solutions to prove that the diffraction shift was not due to interactions between the OP and the amine or carboxyl groups on the polymer backbone, but rather was due to the specific inactivation of the AChE's active site by the OP. No significant shift in the diffraction was observed.

If the response were due to formation of an anionic species which creates a Donnan potential, then no swelling would occur in a high ionic strength environment[29]. We see no response of the AChE-PCCA to parathion in the presence of 150 mM NaCl. Thus, the response is due to the formation of a covalently attached ionic species.

A final control measurement shows that the response at low parathion concentrations is not due to an impurity introduced during the sample preparations. We mimicked the preparation of parathion dilutions, but without using parathion. No diffraction shift occurs in the absence of parathion.

**2.3.4 AChE-PCCA is a dosimetric sensor for organophosphates**

Thus, our sensor mechanism is consistent with the expected mechanism in which parathion phosphorylates the serine residue of the AChE active site.[33] The tetrahedral adduct formed undergoes aging to form a stable anionic species.[17,18] Formation of an anionic charge on the phosphonyl sulfur group causes a Donnan potential inside the AChE-PCCA, which induces a negative osmotic pressure which draws water into the hydrogel matrix.[28,34-36] This forces the hydrogel to swell in low ionic strength solutions. The embedded CCA lattice spacing increases, causing a red-shift in the wavelength of Bragg-diffracted light.

## 2.4 Conclusions

We developed a novel material which can determine femtomolar concentrations of parathion in low-ionic strength aqueous media. This detection limit is ~1 million fold lower than other current detection methods. We are developing this sensor for use in detecting OPs in the field.

A transient sensing approach can be employed to overcome the high ionic strength interference from field samples.[37] The sensor would be exposed to field samples, and then rinsed with deionized water. The OP would remain attached within the sensor

while all other species would wash out. The diffraction wavelength shift of the rinsed

sensor would be proportional to the amount of OP in the original sample.


The AChE sensor should be able to detect numerous OP species, and could be

used for visually monitoring OP levels in groundwater and air.


The sensor response window presently spans the blue-green to orange visible

spectral region. We are working on increasing the spectral window so that it can span the

entire visible spectral region.


### 2.4.1 Acknowledgments

## 2.5 References

(1)     Hopkins, E.H., Hippe, D.J., Frick, E.A., and Buell, G.R., *Organophosphorus pesticide occurrence and distribution in surface and ground water of the United States, 1992-97.* **2000,** U.S. Geological Survey Open File Report 00-187, Denver, CO.

(2)     Radic, Z., Pickering, N.A., Vellom, D.C., Camp, S., and Taylor, P. *Biochem.* **1993**, *32*, 12074-12084.

(3)     Dziri, L., Boussaad, S., Tao, N., and Leblanc, R.M. *Langmuir* **1998**, *14*, 4853-4859.

(4)     Zaugg, S.D., Sandstrom, M.W., Smith, S.G., and Fehlberg, K.M., *Determination of pesticides in water by C-18 solid phase extraction and capillary column gas chromatography/mass spectrometry with selected-ion monitoring.* **1995,** U.S. Geological Survey Open-File Report 95-181, Denver, CO.

(5)     Agency for Toxic Substances and Disease Registry (ATSDR). Toxicological profile for methyl parathion. **2001**, Update. Atlanta, GA: U.S. Department of Health and Human Services, Public Health Service.

(6)     Leon-Gonzalez, M.E.; Townshend, A. *Anal. Chim. Acta*, **1990,** 236, 267-272.

(7)     Marx, S.; Zaltsman, A.; Turyan, I.; Mandler, D. *Anal. Chem.* **2004,** *76*, 120-126.

(8)     Dziri, L.; Boussaad, S.; Tao, N.; and Leblanc, R.M. *Langmuir* **1998**, *14*, 4853-4859.

(9)    Cao, X.; Mello, S.V.; Sui, G.; Mabrouki, M.; and Leblanc, R.M. *Langmuir* **2002**, *18*, 7616-7622.

(10)   Constantine, C.; Mello, S.V.; Dupont, A.; Cao, X.; Santos, D.; Oliveira, O.N.; Strixino, F.T.; Pereira, E.C.; Cheng, T.; Defrank, J.J.; and Leblanc, R.M. *J. Am. Chem. Soc.*, **2003**, *125*, 1805-1809.

(11)   Mello, S.V.; Mabrouki, M.; Cao, X.; Leblanc, R.M.; Cheng, T.; and Defrank, J.J. *Biomacromolecules* **2003**, *4*, 968-973.

(12)   Li, Y., Zhou, Y., Feng, J., Jiang, Z., and Ma, L. *Anal. Chim. Acta,* **1999**, *382*, 277-282.

(13)   Mulchandani, P., Chen, W., and Mulchandani, A. *Environ. Sci. Technol.* **2001,** *35*, 2562-2565.

(14)   Sacks, V., Eshkenazi, I., Neufeld, T., Dosoretz, C., and Rishpon, J. *Anal. Chem.* **2000**, *72*, 2055-2058.

(15)   Burtis, C.A., and Ashwood, E.R. (Eds). Cholinesterases from *Tietz Textbook of Clinical Chemistry,3rd Edition,* **1999**, W.B. Saunders, Philadelphia, 708-711, 939-940.

(16)   Timbrell, J.A., *Principles of Biochemical Toxicology,* **1991,** Taylor and Francis, Washington, D.C.

(17)   Abou-Donia, M.B.; Chang, L.W., and Dyer, R.S. (ed). Organophosphorus Pesticides in *Handbook of Neurotoxicology*, **1995,** Marcel Dekker, Inc. New York, 419-473.

(18)   Millard, C.B.; Kryger, G.; Ordentlich, A.; Greenblatt, H.M; Harel, M.; Raves, M.L.; Segall, Y.; Barak, D.; Shafferman, A.; Silman, I.; Sussman, J.L. *Biochemistry* **1999**, 38, 7032-7039.

(19)   Millard, C.B.; Koellner, G.; Ordentlich, A.; Shafferman, A.; Silman, I.; Sussman, J.L. *J. Am. Chem. Soc.* **1999**, 121, 9883-9884.

(20)   Asher, S.A. Flaugh, P.L.; Washinger, G. *Spectroscopy* **1986**, *1*, 26-31.

(21)   Carlson, R.J.; Asher, S.A. *Appl. Spectrosc.* **1984**, *38*, 297-304.

(22)   Weissman, J.M.; Sunkara, H.B.; Tse, A.S.; Asher, S.A. *Science* **1996**, *274*, 959-960.

(23)   Reese, C.E.; Guerrero, C.D.; Weissmann, J.M.; Lee, K.; Asher, S.A. *J. Coll. Interface. Sci.* **2000**, *232*, 76-80.

(24)   Flaugh, P.L.; O'Donnell, S.E.; Asher, S.A. *Appl. Spectrosc.* **1984**, *38*, 847-850.

(25)   Rundquist, P.A.; Photinos, P.; Jagannathan, S.; Asher, S.A. *J. Chem. Phys.* **1989**, *91*, 4932-4941.

(26)   Asher, S.A.; Holtz, J.; Liu, L.; Wu, Z.; *J. Am. Chem. Soc.* **1994**, *116*, 4997-4998.

(27)   Holtz, J.H.; Asher, S.A. *Nature* **1997**, *389*, 829-832.

(28)   Holtz, J.H.; Holtz, J.S.; Munro, C.H; Asher, S.A. *Anal. Chem.* **1998**, *70*, 780-791.

(29)  Asher, S.A.; Holtz, J.H.; Weissman, J.M.; Pan, G. *MRS Bull.* **1998**, (October), 44-50.

(30)  Inman, J.K.; Dintzis, H.M. *Biochem.* **1969**, *8,* 4074-4082.

(31)  Ellman, G.L.; Courney, K.D.; Andres, V.; Featherstone, R.M. *Biochem. Pharmacol.* **1961**, *7*, 88-95.

(32)  Sussman, J.L., Harel, M., Frolow, F., Oefner, C., Goldman, A., Toker, L., and Silman, I. **1991**, *Science 253*, 872-879.

(33)  Wilson, I.B. **1951**, *J. Biol. Chem. 190*, 111-117.

(34)  Dusek, K. **1993**, (ed) Responsive gels: volume phase transitions, Advances in polymer science *109*. Springer, Berlin

(35)  Dusek, K. **1993**, (ed) Responsive gels: volume phase transitions II, Advances in polymer science *110*. Springer, Berlin.

(36)  Lee, K.; Asher, S.A. *J. Am. Chem. Soc.* **2000**, *122*, 9534.

(37)   Reese, C.E.; Asher, S.A. *Anal. Chem.* **2003**, *75*, 3915-3918.

## Photonic Crystal Sensor for Organophosphate Nerve Agents Utilizing the Organophosphorus Hydrolase Enzyme

## 3.1 Introduction

Synthetic organophosphorus compounds (OPs), such as parathion and paraoxon, are widely used agriculturally in both the United States and worldwide as pesticides and insecticides.[1] These compounds are also structurally similar to chemical warfare agents (CWAs) such as sarin, soman and VX. OP compounds are commonly found in agricultural wastes at levels between 1 – 10,000 ppm.[1] These compounds are potent inhibitors of the enzyme acetylcholinesterase (AChE), because they prevent breakdown of the neurotransmitter acetylcholine at the neural synapse.[2] The inhibition of acetylcholine breakdown and subsequent accumulation results in loss of muscular function and can result in paralysis or death if untreated.[3,4] Due to the widespread use of these agents in agriculture, a high risk of food and ground water contamination exists. The neurotoxicity of OP compounds is of immense concern, given their potential for use in chemical terrorism. Due to this threat, there is intense interest in developing sensors which can rapidly and selectively detect OP compounds for environmental analysis as well as for military/ law enforcement applications such as counter terrorism and battlefield detection of OP agents. Rapid detection is a crucial element for preventive response, exposure treatment, and decontamination.

Several types of techniques exist for detection and identification of OPs. Thin layer chromatography, HPLC and GC/MS techniques are commonly used and provide nanomolar detection limits.[5,6] These techniques are, however, expensive and time consuming, requiring significant sample preparation and skilled technicians for operation, which limits their practical use in field detection. Molecularly imprinted polymers (MIPs) which have very high selectivity towards OP substrates have also been developed. These sol-gel films utilize silanes which are functionalized to create OP-binding templates. Detection of the sequestered OP molecules is done using fluorescence or electrochemistry.[7]

Recent research has focused on developing sensors which utilize biological recognition elements such as enzymes to detect and quantify OPs. These sensors provide a significant advantage over current chemical sensing techniques because they utilize specific enzymes which have very high affinities for OP analytes. For example, AChE and Organophosphorus Hydrolase (OPH, also called phosphotriesterase) have been extensively utilized in biosensor development.

AChE is inhibited by OPs at the catalytic serine site, which prevents turnover of acetylcholine at the neural synapse.[2] Several sensors utilize AChE either by directly using it to bind an OP and measuring the sensor's response, or by measuring changes in the amount of substrate turnover caused by exposure to OPs.[8-12] A flow injection technique utilizing immobilized AChE has been developed where AChE is immobilized on a polymer substrate.[8] A sample solution containing OP is then exposed to the immobilized

enzyme. A solution containing an enzyme substrate and reagent which reacts to form a chromophore upon substrate catalysis is added. The absorbance of the chromophore is monitored to detect changes in enzyme activity caused by OP inihibition. Leon-Gonzalez and Townshend achieved 8 nM OP detection limits with this technique.[8]

Langmuir-Blodgett multilayer sensors have also been developed utilizing AChE along with several other recognition elements. These sensors, which monitor changes in fluorescence caused by OP binding, also achieved nM detection limits.[9,10] Amperometric sensors have also been fabricated which utilize AChE to detect very low OP concentrations.[11] These techniques can be easily miniaturized and are less expensive. Thus, they are more suitable for field detection than most other types of sensors. However, they are subject to interference from the other oxidizable substances present in real samples.[11] A piezoelectric sensor which monitors the binding of cholinesterase to inhibitors using a mass-sensitive quartz crystal was also recently developed. The sensor is capable of detecting $10^{-10}$ M paraoxon.[12]

We previously demonstrated a photonic crystal sensor which acts as a dosimeter and which operates in low ionic strength solution that detects OPs based on a change in the ionic free energy of the system due to creation of a charged species that forms when parathion inhibits AChE.[13] Binding of OP shifts the wavelength of visible light Bragg diffracted by the PCCA. This sensor achieves unprecedented (fM) detection limits; however it only works in low-ionic strength solution, and, thus, is not ideally suited for use in real samples.

Sensors which utilize AChE are fundamentally limited in their development for two primary reasons. First, AChE can be irreversibly inhibited by several other species, such as carbamates and some neurotoxins[7]. These interferences could cause false positive results for OP detection. Alternatively, they could cause false negatives by preventing OP binding to AChE altogether. Secondly, AChE is irreversibly inhibited by OPs[7], so sensors are not continuous or reusable, which increases the cost of performing the analysis. In light of these limitations, researchers have begun to explore the utility of other enzymes for OP detection.

Several researchers have utilized the recombinant enzyme organophosphorus hydrolase (OPH) instead. The development of the recombinant enzyme has facilitated the development of sensors which take advantage of this enzyme's unique properties. OPH is a $\sim$ 35 kDa protein normally present as a homodimer. OPH contains a divalent metal ion cofactor (usually $Zn^{2+}$ or $Co^{2+}$) which catalyzes the hydrolysis of OP esters at pH 8-10, releasing two protons in the process.[14-16] The enzyme is not subject to as significant a degree of interference from other species as is AChE, which can be inhibited by carbamates in addition to OPs. Another advantage of OPH is that it is a recombinant enzyme; researchers have altered the sequence of the enzyme through site-directed mutagenesis in order to produce OPH species which catalyze specific OP species more efficiently.[17] The catalytic reaction of OPH is illustrated in Scheme 1.
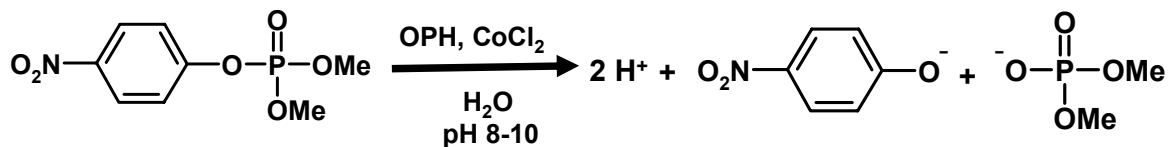
**Scheme 1**: **OPH hydrolyzes methyl-paraoxon, an organophosphorus pesticide, into p-nitrophenolate and dimethylphosphate at basic pH, producing two protons in the process.**

Several types of sensors which utilize OPH have been developed. Potentiometric sensors based on measuring the pH changes caused by the OPH catalyzed degradation of OP species have been developed.[16,18,19] For example, Mulchandani et.al. reported a 2 $\mu$M detection limit with one such system.[16] Amperometric sensors utilizing OPH have also been developed.[,20,21,22,23] These sensors oxidize p-nitrophenol, a paraoxon hydrolysis product, which is then detected at a carbon paste electrode. Detection limits as low as 20 nM have been demonstrated.[21] Another sensor employed a bacterium which oxidizes 2-nitrophenol to $CO_2$, consuming $O_2$ in the process. The $O_2$ consumed, measured by an oxygen electrode, correlates with the concentration of OP present. The detection limit for this technique was reported to be 0.2 $\mu$M OP.[23]

OPH has also been recently utilized not only for sensing applications, but also for decontamination of OP-containing samples.[24,25] Current chemistry-based decontamination techniques frequently require use of caustic materials, however these strong alkalis can damage the contaminated objects as well as the environment.[25] OPH can eliminate use of caustics because it selectively hydrolyzes OP species. The possibility of producing multi-use reversible enzymatic systems capable of OP detection and

decontamination would provide a significant advantage for anti-terrorism preparedness and for contaminant clean-up. Such systems would provide a rapid, cost-effective single approach for initial detection, decontamination, and the monitoring of the decontamination process.

We demonstrate in this paper the development of a novel, inexpensive sensor for detection of OP species based on our previously developed intelligent polymerized crystalline colloidal array (IPCCA) photonic crystal sensing materials. These IPCCAs utilize an array of colloidal particles[26-31] polymerized into a hydrogel[32-35] network which Bragg diffracts light in the visible spectral region. We utilize our recently-developed general bimodular sensing motif originally demonstrated for sensing creatinine.[36] The first sensing element is an enzyme, which reacts with the analyte to produce a steady-state pH gradient inside the hydrogel. The pH change is then detected by the second sensing element, which titrates to cause a sensing response.

Our OP-sensing IPCCA contains OPH, which degrades the OP methyl-paraoxon to p-nitrophenolate and dimethylphosphate at pH 9.7, producing two protons. These protons protonate the secondary sensing element, 3-aminophenolate (3-AMP), causing a steady-state volume change in the PCCA. The wavelength of diffracted light shifts in response to the steady-state volume change of the hydrogel. Figure 1 illustrates this sensing motif.
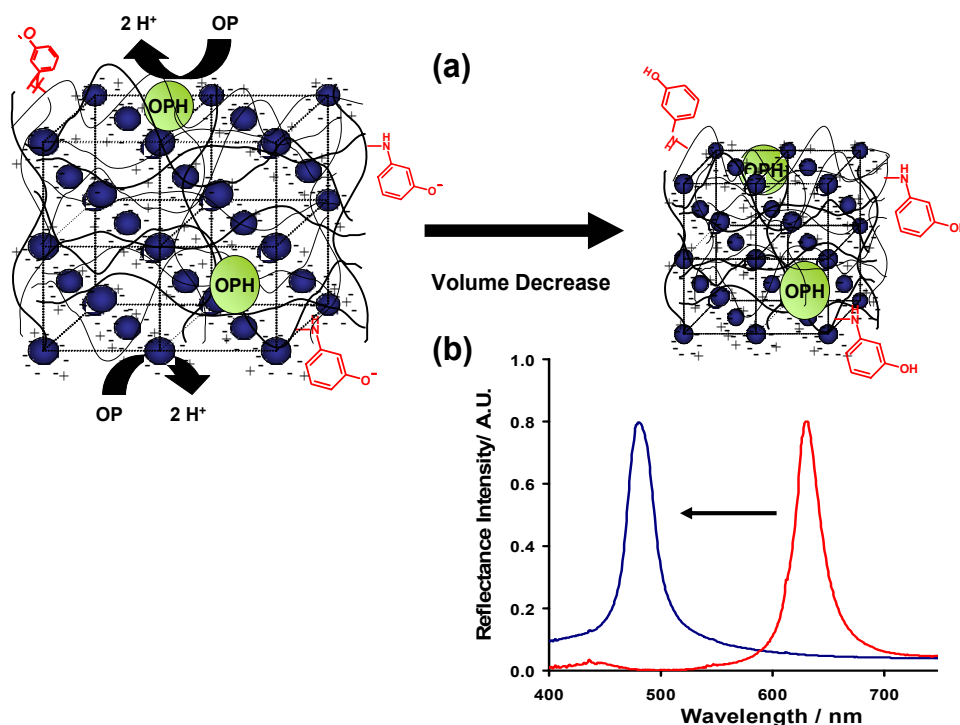
**Figure 1: a) CCAs form due to electrostatic repulsion between particles. The particle spacing is such that the array Bragg diffracts visible light. The lattice is locked into place by a poly-2-hydroxyethylacrylate hydrogel network. The backbone is functionalized with both organophosphorus hydrolase (OPH) and 3-aminophenolate. As OPH reacts with methyl-paraoxon, p-nitrophenolate and dimethylphosphate, as well as two protons are produced. This produces a steady-state pH gradient between the interior and exterior regions of the hydrogel. The lower pH inside the hydrogel protonates the phenolates. As a result, the solubility of the hydrogel network decreases, which shrinks the hydrogel and blue-shifts the IPCCA diffraction. b) The diffraction peak of the IPCCA blue-shifts in response to the analyte concentration.**

Our PCCA sensor platform relies upon a volume phase transition phenomenon which occurs in the hydrogel matrix due to changes in the free energy of the system. For this sensor, the volume change is caused by a change in the free energy of mixing ($\Delta G_{mix}$) of the hydrogel.[37] The back-diffracted light follows Bragg's Law:

$$\lambda_o = 2\, n\, d\, \sin\theta$$

The wavelength ($\lambda_o$) of light diffracted by the IPCCA's 111 plane of the fcc lattice depends upon the plane spacing (*d*), the refractive index (*n*) of the system, and the Bragg glancing angle, $\theta$. Because we are sampling normally incident light, sin $\theta$ is unity. We demonstrate that our sensor reversibly detects the OP pesticide methyl-paraoxon at submicromolar concentration levels in lab buffer solution as well as in stream water samples.

## 3.2 Experimental

### 3.2.1 PCCA Preparation

Figure 2 depicts the synthesis and functionalization of the OP IPCCA sensor. 2-hydroxyethylacrylate (2-HEA, 0.94 g, 8.1 mmol, Sigma), acrylamide (AMD, 0.02 g, 0.28 mmol, Fluka), polyethylene glycol (200) dimethacrylate (PEGDMA-200, 0.09 g, 0.25 mmol, Polysciences), glycidyl acrylate (GA, 0.04 g, 0.37 mmol, Sigma) and ethylene glycol (1.95 g, 31 mmol, J.T. Baker) were mixed and treated with $Al_2O_3$ to remove inhibitors from the monomers. The mixture was centrifuged to separate the monomer from the $Al_2O_3$. 1.015 g of this solution was mixed with the colloid suspension (1.0 g, 5-10% w/w dispersion, polystyrene latex spheres, 120 nm).[26-31] AG501-X8 (D) ion exchange resin (~ 0.1 g, 20-50 mesh, mixed bed, Bio-Rad) and 10 % diethoxyacetophenone (DEAP, 10 µL, 4 µmol, Aldrich) in dimethylsulfoxide (DMSO, J.T. Baker) were mixed into the suspension in a 2-dr vial.  After 15 min, the mixture was centrifuged to remove the ion-exchange resin and was injected between two quartz discs separated by a 125 µm-thick Parafilm spacer. The colloidal particles self-assemble into a

crystalline colloidal array (CCA), resulting in a liquid film which diffracts light. The film

was exposed to 365 nm UV light from mercury lamps (Blak Ray) for 3 hrs. A poly-2-

HEA/AMD hydrogel network with PEGDMA cross-links forms around the CCA,

resulting in a polymerized CCA (PCCA).[32-35] The quartz cell enclosing the hydrogel was

opened in Nanopure water and the PCCA was allowed to equilibrate with water.
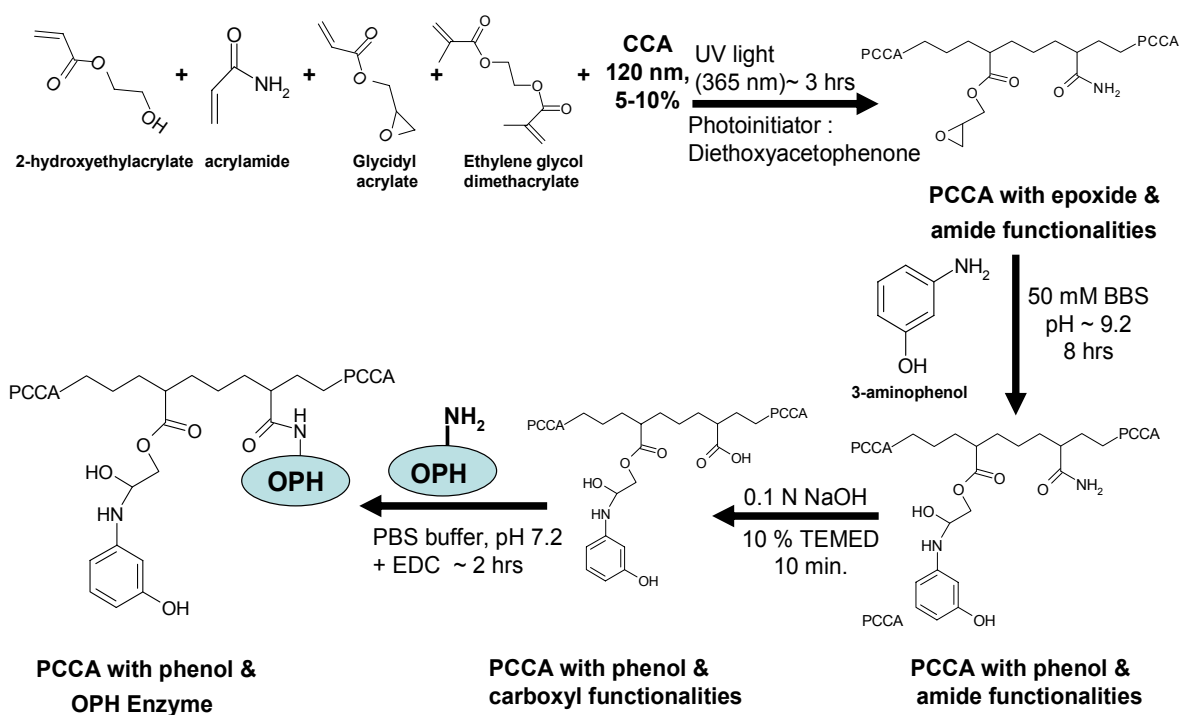


**Figure 2: Preparation of the IPCCA and functionalization with 3-aminophenol and OPH. The 3-AMP is first coupled via epoxide ring opening. The pendant amides are subsequently hydrolyzed to form carboxylates, which are carbodiimide-coupled to amines on the OPH enzyme.**

### 3.2.2 Attachment of 3-Aminophenol

The PCCA was placed into a 50 mM borate buffer solution (BBS, pH 9.2, J.T. Baker) to

equilibrate before coupling. 0.5 g of 3-aminophenol (3-AMP, 4.6 mmol, Sigma) were

46

dissolved in 10 ml DMSO (J.T. Baker) and then diluted to 50 ml with 50 mM BBS. The solution and PCCA were placed in a 125 ml plastic container (Nalgene) and allowed to react for 8 hours. After reacting, the PCCA was rinsed hourly for 6 hours with BBS. A blank gel (hydrogel in which CCA is replaced with $H_2O$) was prepared and functionalized according to the above protocol. UV-VIS spectra of the blank gel were measured by a Varian Cary 5000 UV-VIS spectrophotometer to confirm attachment of 3-AMP by monitoring the absorbance at 290 nm. The sensor typically contains a 13 mM concentration of 3-AMP.

### 3.2.3 Attachment of Organophosphorus Hydrolase

The PCCA was then hydrolyzed in a 50 mL solution of NaOH (0.1 M, J.T. Baker) containing 10 % v/v N,N,N',N'-tetramethylethylenediamine (TEMED, Aldrich) for 10 min. The hydrolyzed PCCA was washed for 2 hrs with 150 mM NaCl (J.T. Baker). UV-VIS Spectra were recorded to confirm that phenols remained attached to the hydrogel after hydrolysis.

A piece of the PCCA (1 cm x 1 cm x 125 μm) was allowed to adhere to a plastic petri dish (Falcon). A coupling solution of enzyme was made by dissolving 6 mg Organophosphorus Hydrolase (OPH, EC 3.1.8.1., 6 mg solid, MW 35,000, Lybradyn, Inc.) in 200 μL of 0.1 M phosphate buffer (PBS, Pierce Biotechnology). The PCCA was incubated overnight in the enzyme solution to allow the OPH to diffuse into the hydrogel. Next, 0.1 g of 1-ethyl-3-(3-dimethylaminopropyl) carbodiimide hydrochloride (EDC,

0.52 mmol, Pierce Bitoechnology) was dissolved into 100 µL of 0.1 M 2-(N-morpholino)ethanesulfonic acid (MES, pH 4.7, Pierce Biotechnology). The EDC solution was added, and the reaction was allowed to proceed for 2 hrs. The sensor was rinsed in 150 mM NaCl (J.T. Baker) and stored overnight until testing in 0.1 M PBS solution at 4$^o$C. UV-VIS spectra were also recorded for a blank hydrogel treated exactly the same way. OPH attachment was confirmed by monitoring the absorption difference spectrum of the blank hydrogel functionalized with 4-amino-2-nitrophenol instead of 3-AMP. The absorption difference spectrum was generated by subtracting spectra of the sample before and after coupling.

### 3.2.4 Solutions & Diffraction Measurements

The PCCA was stored in 0.1 M PBS (pH 7.4) at 4$^o$C at all times when not being tested. We made the following buffer test solution (BTS) which contained: 2 mM Na$_2$B$_4$O$_7$·10 H$_2$O (J.T. Baker), 5% v/v methanol (Fisher), 0.05 mM CoCl$_2$·6H$_2$O (Fisher), and 150 mM NaCl (J.T. Baker). The test solution pH was adjusted to ~9.7 with 0.1 M NaOH (Fisher).

The PCCA diffraction was monitored using a fiber-optic diode spectrometer with a tungsten halogen light source (Ocean Optics) using a reflectance probe. All measurements were conducted with the PCCA adhering to the bottom of the petri dish with stirring using a magnetic stir bar.

The sensor was first titrated to confirm that the 3-AMP was attached and that the sensor responded to titration of the attached phenols with 20 mM NaOH (Fisher). We used these data to confirm the $pK_a$ of the attached phenols.

We then tested the sensor with a control as well as in a series of BTS dilutions of the OP pesticide methyl-paraoxon (ChemService, Inc.) ranging in concentration from 2.4 µM to 1 mM. The IPCCA was pre-equilibrated in BTS for 30 min. prior to exposure to the methyl-paraoxon solutions. Diffraction spectra were recorded until the diffraction stopped shifting, indicating that the sensor had reached steady-state. Responses typically were saturated in about 50 min. The sensor was subsequently rinsed and re-equilibrated in BTS. The sensor was subsequently exposed to a new methyl-paraoxon solution. Two sensing runs were performed with the sensor on consecutive days. We utilized the range of concentrations from 0 – 24 µM methyl-paraoxon to calculate the detection limit.

We also performed several control experiments in order to confirm that the response was due to a change in the free energy of mixing of the PCCA. We tested the sensor with various components absent in order to prove that the sensing response was produced by titration of the pendant phenolates by the protons produced during the OPH hydrolysis of methyl-paraoxon. Several control studies were also performed to confirm the hypothesis that the sensor displays a steady-state response and not an equilibrium response.

Finally, the response of the sensor was tested in stream water to determine the sensor performance in a real sample matrix. Water samples were obtained in July, 2006 from a small stream behind the Plantations housing development in Saxonburg, PA. The the sample was first filtered through a 2 μm filter to remove particulate matter. Then, the stream water samples were prepared by adding 5% (v/v) methanol to help solubilize the OP,150 mM NaCl, 0.05 mM $CoCl_2 \cdot 6H_2O$, 2 mM $Na_2B_4O_7 \cdot 10 \ H_2O$, and adjusting the pH to 9.7 with 0.1 M NaOH. This solution was used in place of the BTS to make serial dilutions of methyl-paraoxon via the protocol used previously.

## 3.3 Results & Discussion

### 3.3.1 UV-VIS Confirmation of Sensing Element Attachment

The conjugation of 3-AMP and OPH to the hydrogel matrix was monitored on a colloid-free hydrogel (blank gel) through absorption spectroscopy (Fig. 3). Each sensor was rinsed for several hours with 150 mM NaCl solutions to remove unreacted species. The 3-AMP is initially present at a concentration ~ 25 mM, but the hydrolysis step necessary for coupling OPH also hydrolyzes some of the ester bonds between the phenolate and the hydrogel, leaving ~ 13 mM phenol attached to the hydrogel (Fig. 3a). OPH attachment to a blank hydrogel was confirmed by monitoring the tyrosine/tryptophan absorbance at 280 nm. Prior to OPH coupling, 4-amino-2-nitrophenol, which does not have an absorbance maximum at 280 nm, was attached to the blank hydrogel instead of 3-AMP. Thus spectral overlap between OPH and 3-AMP was avoided. Fig. 3b. displays the difference spectrum of the blank hydrogel before and after

OPH coupling. Using the extinction coefficient of the OPH monomer, 26,740 $M^{-1}cm^{-1}$ at 280 nm,[38] we calculated an 8 µM OPH concentration in the hydrogel using the difference spectrum.

We also proved that OPH was attached to the sensor by monitoring the 412 nm absorbance of p-nitrophenol, an OP hydrolysis product, in BTS containing methyl-paraoxon, and found that the rate of hydrolysis was ~ 400 times greater in the presence of an OPH-functionalized PCCA than in the presence of a PCCA lacking OPH. The OPH hydrolysis rates are typically 40-2450 times faster than in a 0.1 N NaOH solution.[39] This result also demonstrates that functional OPH is attached to the PCCA.
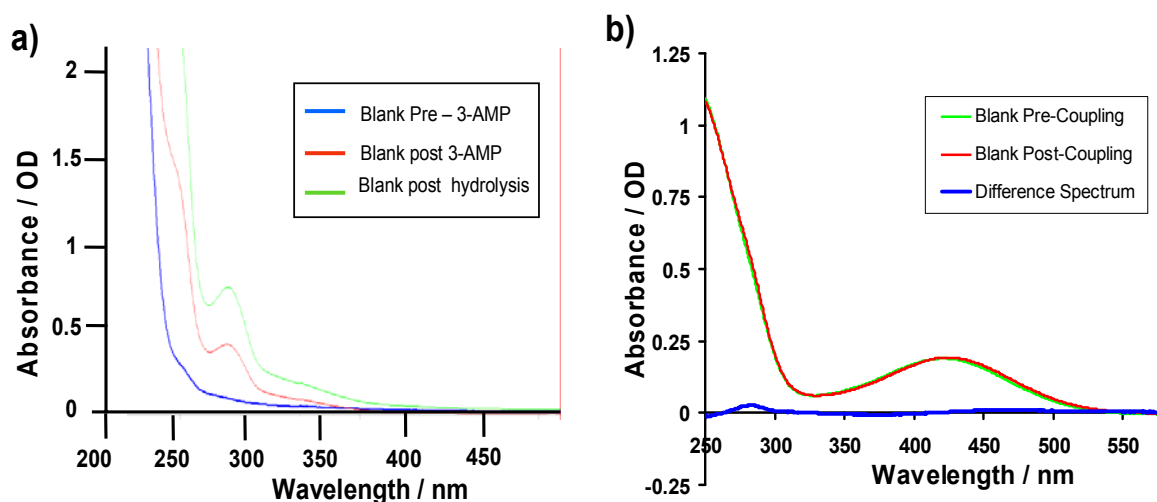


**Figure 3: UV-VIS absorbance spectra of CCA-free hydrogels. a) displays the spectra at various stages of 3-AMP coupling. The blue line is the spectrum of a blank poly-2-HEA hydrogel prior to conjugation, the green spectrum is the blank after coupling with 3-AMP, and the red spectrum is after hydrolysis and rinsing. b) shows the spectra of a poly-2-HEA hydrogel with 4-amino-2-nitrophenol attached before (green) and after (red) OPH coupling. The blue difference spectrum represents the absorbance difference after coupling OPH. The peak at ~ 280 nm in the difference spectrum indicates OPH attachment. 4-amino-2-nitrophenol, which absorbs at ~ 430 nm instead of ~280 nm, was coupled instead of 3-AMP in order to avoid dominating overlap between the absorbance peaks of 3-AMP and OPH.**

### 3.3.2 PCCA Titration in Test Buffer

We monitored the diffraction of the PCCA with 3-AMP attached in BTS in order to determine the $pK_a$ of the phenol groups, which should be close to the $pK_a$ of 3-acetamidophenol (Fig. 4). Both the borate buffer ($pK_a = 9.2$) and the 3-acetamidophenol ($pKa = 9.65$) groups titrate at their expected $pK_a$ values.[40] We observed that when the pH rises above the inflection point of the buffer, the sensor diffraction wavelength shifts. We conclude that the response is due to the deprotonation of the phenols, which makes the free energy of mixing of the hydrogel more favorable.[37] The titration and diffraction measurements show inflection points at pH ~ 9.6, the $pK_a$ of the conjugated phenol. These measurements were repeated on the same PCCA after rinsing to demonstrate reproducibility and reversibility of the response.
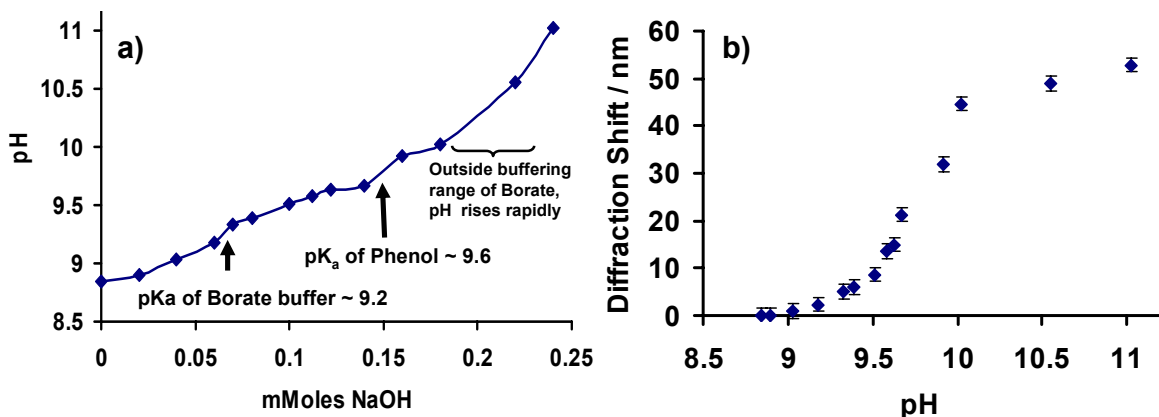


**Figure 4: a) The solution pH versus the number of millimoles NaOH added. The $pK_a$ of the borate buffer (pH ~ 9.2) and the 3-AMP (pH ~ 9.6) are apparent. b) Diffraction red-shift of the PCCA as a function of the pH. We see that while the titration of the buffer occurs, there is very little response from the PCCA. But, as the phenol groups are titrated, we see the PCCA diffraction red-shifts. The inflection point in (b) occurs at the phenolate $pK_a$, indicating that the diffraction response is due to the phenol titration.**

### 3.3.3 Dependence of PCCA Diffraction on Methyl-Paraoxon Concentration

Our IPCCA organophosphate sensor contains both 3-aminophenol and OPH, which catalyzes the hydrolysis of methyl-paraoxon and releases protons.[16] The products, p-nitrophenol and dimethyl hydrogen phosphate, have pK$_a$ which are lower than the buffered solution pH of 9.2 (7.22 and 1.24, respectively)[40] and thus decrease the internal pH of the IPCCA and protonates the pendant phenolates. This causes a steady-state reduction in the free energy of mixing, causing the gel to shrink. This volume change blue-shifts the diffraction in proportion to the concentration of methyl-paraoxon.

Fig. 5 shows the methyl-paraoxon concentration dependence of our IPCCA sensor diffraction in BTS. The diffraction wavelength blue-shifts with increasing concentration of methyl-paraoxon. The shift essentially saturates by 240 μM methyl-paraoxon. At lower concentrations (≤24 μM) the response is quite linear, so a detection limit can be calculated. This concentration range is shown in the inset of Fig. 5a. The detection limit is determined by the concentration of analyte that gives a response equal to 3 standard deviations of the blank. We calculate a 0.2 μM detection limit. Some AChE-based sensors achieved lower detection limits (typically 1-10 nM) because AChE irreversibly binds OPs and/or because AChE shows an extremely fast hydrolysis rate. Our current reversible sensor achieves the same level of detection as OPH-based biosensors based on potentiometry.[16,18,19] However, these new IPCCA OP sensors based on OPH are reversible, as evident by our use of the same sensor for replicate measurements.
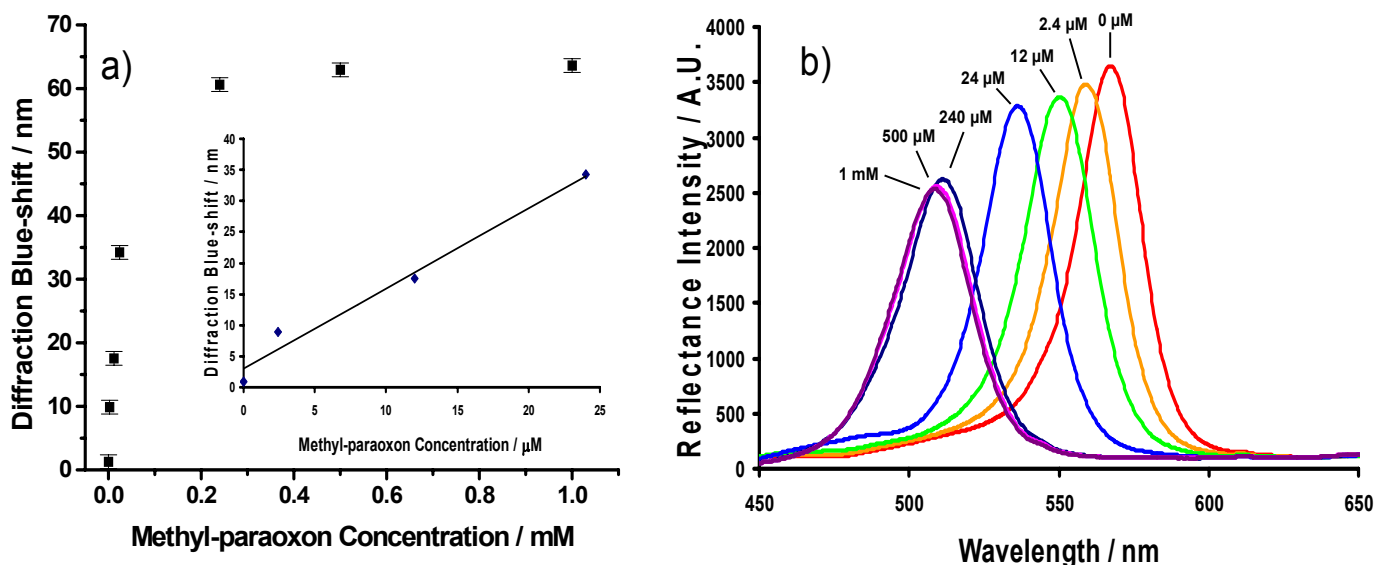
**Figure 5: a)The PCCA diffraction wavelength as a function of methyl-paraoxon concentration in BTS. Inset is the range (0-24 µM methyl-paraoxon) used to calculate the limit of detection. b) shows the representative diffraction spectra of the PCCA at several methyl-paraoxon concentrations. The standard error in the measurement was σ = 1.1 nm for 2 replicates.**

### 3.3.4 Confirmation of Sensing Mechanism

Sharma et.al. previously demonstrated a similar bimodular sensing approach utilizing the PCCA sensing platform in which a hydroxide enzyme hydrolysis product titrated a phenol, producing a steady-state pH gradient between the interior and exterior of the hydrogel, which changed the free energy of mixing, producing a diffraction wavelength shift proportional to the analyte concentration.[36] We performed several control experiments which confirmed that our sensor was also bimodular and responded to analyte through a decrease in the free energy of mixing of the hydrogel produced by the steady-state pH gradient within the sensor, which titrates pendant phenolates.

We also tested the sensor with OP in the absence of either 3-AMP or OPH to prove that the sensing response was due to a bimodular motif. The PCCA functionalized with OPH, but lacking 3-AMP showed only a small ~1 nm diffraction wavelength blue-shift for 240 µM methyl-paraoxon.

A PCCA with 3-AMP and no OPH attached was also exposed to a 240 µM methyl-paraoxon solution. Under these conditions, the sensor actually blue-shifted ~ 3 nm after 60 minutes. This is very small compared to the normal sensing response of the IPCCA with OPH attached (~ 62 nm). This small blue-shift may result from the slow hydrolysis of methyl-paraoxon in the basic solution, catalyzed by the hydrogel. The hydrolysis produces a few protons that cause the gel to shrink slightly.

We performed studies to confirm that the sensing response resulted from a steady-state response and not an equilibrium response. We monitored the absorbance of a 12 µM methyl-paraoxon in BTS solution exposed to an OPH-functionalized IPCCA via UV-VIS of the solution in order to calculate the rate of production of p-nitrophenol, which absorbs at 412 nm. Using the rate of the p-nitrophenol absorbance increase, we calculated that it would take over 3 hrs for the sensor to hydrolyze all of the methyl-paraoxon. However, our sensor achieves full response in 50 minutes and thereafter remains stable for over an hour (Fig. 6). After 2 hrs, the sensor begins to red-shift back towards the starting diffraction. We observed a similar response for 2.4 µM methyl-paraoxon concentration.

This response plateau occurs because the sensor reaches a steady-state after about 1 hr where the rate of $H^+$ diffusion out of the gel is equal to the rate of $H^+$ production from the OPH-mediated hydrolysis of methyl-paraoxon. After 2 hrs, the 12 µM methyl-paraoxon is depleted by the enzyme, and the sensor subsequently red-shifts. Our observations are consistent with the steady-state bimodular results reported by Sharma et. al.[36]
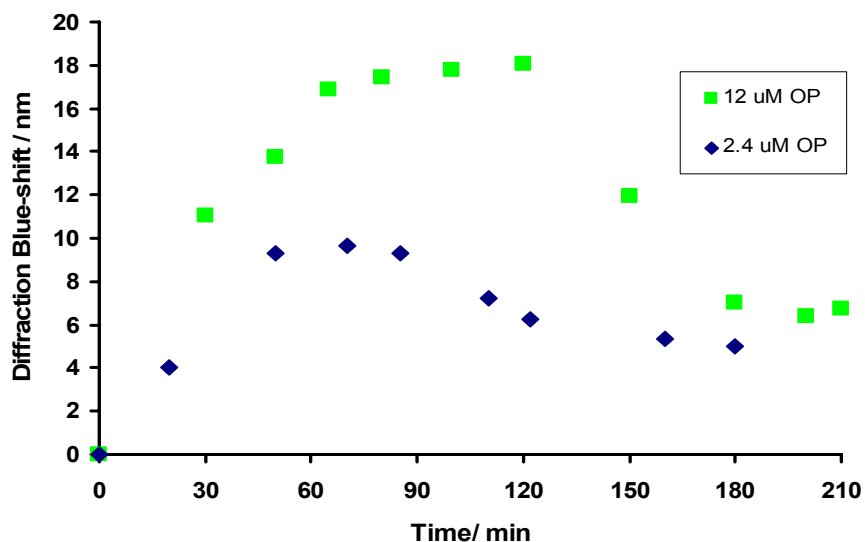


**Figure 6: Time dependence of the diffraction blue shift at two different methyl-paraoxon concentrations. Steady-state is established within ~ 60 min. The diffraction red-shifts at longer times due to depletion of the analyte.**

### 3.3.5 Stream Water Testing

We exposed the same sensor to both methyl-paraoxon in BTS as well as in a prepared stream water sample to compare the response of the sensor to laboratory

samples and to environmental samples (Fig. 7). The sensor displays a blue-shift of ~ 52 nm in response to 1 mM OP in BTS solution, compared to a blue-shift of ~ 46 nm to 1 mM OP in the stream water sample. The responses in stream water are consistently about 16 % smaller than in BTS at concentrations above saturation (>250 µM OP).

In order to determine why the spectral window is reduced in stream water, we titrated the stream water sample to determine whether there was another natural buffer present, such as calcium carbonate, which would increase the effective buffer concentration and reduce the spectral window of the sensor. The stream water did not require much base to increase the pH significantly, and no inflection point was found. The spectral window was not reduced by the presence of a natural buffer.



**Figure 7: PCCA OP sensor diffraction wavelength as a function of methyl-paraoxon pesticide concentration in both BTS and filtered stream water. The sensor displays a 16% smaller response in stream water compared to its response in BTS. The inset shows the concentrations ≤ 24 µM methyl-paraoxon.**

A possible cause for the reduction in the spectral window in real samples is the presence of other species which function as OPH inhibitors, which could cause the OPH

to turn over the methyl-paraoxon at a slower rate. A slower turnover rate would decrease the steady-state pH gradient, which would cause less protonation of the phenolates, which would result in a smaller diffraction blue-shift.

## 3.4 Conclusions

We developed a sensor which is capable of determining submicromolar concentrations of the organophosphate pesticide methyl-paraoxon. Organophosphorus hydrolase enzyme immobilized inside the hydrogel catalyzes the hydrolysis of methyl-paraoxon, producing protons which create a steady-state pH gradient in the hydrogel. Pendant phenolates are protonated as a result of this pH gradient, causing a decrease in the free energy of mixing of the hydrogel, which shrinks the gel and blue-shifts the wavelength of light diffracted by the CCA proportional to the concentration of OP in solution. The OPH-based photonic crystal sensor operates at high ionic strength and is reversible, so that it can be used as a continuous sensor for environmental sample solutions. We observe submicromolar detection limits in buffer solution and in a stream water sample. We demonstrated that our sensor works in environmental samples by sensing methyl-paraoxon in stream water solutions. We are currently working to increase the spectral window to span the entire visible region and to increase the sensitivity and speed of the sensor response.

### 3.4.1 Acknowledgments

58

## 3.5 References

(1)    Hopkins, E.H.; Hippe, D.J., Frick, E.A.; Buell, G.R. *Organophosphorus pesticide occurrence and distribution in surface and ground water of the United States, 1992-97.* **2000,** U.S. Geological Survey Open File Report 00-187, Denver, CO.

(2)    Burtis, C.A.; Ashwood, E.R. (Eds). Cholinesterases from *Tietz Textbook of Clinical Chemistry,3$^{rd}$ Edition,* **1999**, W.B. Saunders, Philadelphia, 708-711, 939-940

(3)    Radic, Z.; Pickering, N.A.; Vellom, D.C.; Camp, S.; Taylor, P. *Biochem.* **1993**, *32*, 12074-12084.

(4)    Dziri, L.; Boussaad, S.; Tao, N.; Leblanc, R.M. *Langmuir* **1998**, *14*, 4853-4859.

(5)    Zaugg, S.D.; Sandstrom, M.W.; Smith, S.G.; Fehlberg, K.M. *Determination of pesticides in water by C-18 solid phase extraction and capillary column gas chromatography/mass spectrometry with selected-ion monitoring.* **1995,** U.S. Geological Survey Open-File Report 95-181, Denver, CO.

(6)    Agency for Toxic Substances and Disease Registry (ATSDR). Toxicological profile for methyl parathion. **2001**, Update. Atlanta, GA: U.S. Department of Health and Human Services, Public Health Service.

(7)    Marx, S.; Zaltsman, A.; Turyan, I.; Mandler, D. *Anal. Chem.* **2004,** *76*, 120-126.

(8)    Leon-Gonzalez, M.E.; Townshend, A. *Anal. Chim. Acta,* **1990,** 236, 267-272.

(9)    Constantine, C.; Mello, S.V.; Dupont, A.; Cao, X.; Santos, D.; Oliveira, O.N.; Strixino, F.T.; Pereira, E.C.; Cheng, T.; Defrank, J.J.; Leblanc, R.M. *J. Am. Chem. Soc.*, **2003**, *125*, 1805-1809.

(10)   Mello, S.V.; Mabrouki, M.; Cao, X.; Leblanc, R.M.; Cheng, T.; Defrank, J.J. *Biomacromolecules* **2003**, *4*, 968-973.

(11)   Sacks, V.; Eshkenazi, I.; Neufeld, T.; Dosoretz, C.; Rishpon, J.  *Anal. Chem.* **2000**, *72*, 2055-2058.

(12)   Halamek, J.; Pribyl, J.; Makower, A.; Skladal, P.; Scheller, F.W. *Anal. Bioanal. Chem.* **2005,** *382*, 1904-1911.

(13)   Walker, J.P., Asher, S.A. *Anal. Chem.* **2005**, *77*, 1596-1600.

(14)   Lai, K., Dave, K.L., and Wild, J.R. *J. Biol. Chem.* **1994**, *24*, 16579-16584.

(15)   Donarski, W. J.; Dumas, D.P.; Heitmeyer, D.P.; Lewis, V.E.; Raushel, F.M. *Biochem.* **1989**, *28*, 4650-4655.

(16)   Mulchandani, P.; Mulchandani, A.; Kaneva, I.; Chen, W. *Biosens. Bioelectron.* **1999**, *14*, 77-85.

(17)   Cho, C.M.; Mulchandani, A.; Chen, W. *Appl. Environ. Microbiol.* **2004**, *70*, 4681-4685.

(18)   Rogers, K.R.; Wang, Y.; Mulchandani, A.; Mulchandani, P.; Chen, W. *Biotechnol. Prog.* **1999**, *15*, 517-521.

(19)   Rainina, E.; Efremenco, E.; Varfolomeyev, S.; Simonian, A.L.; Wild, J.R. *Biosens. Bioelectron.* **1996**, *11*, 991-1000.

(20)  Mulchandani, A.; Mulchandani, P.; Chen, W.; Wang, J.; Chen, L. *Anal. Chem.* **1999**, *71*, 2246-2249.

(21)  Mulchandani, P.; Chen, W.; Mulchandani, A. *Environ. Sci. Technol.* **2001**, *35*, 2562-2565.

(22)  Lei, Y.; Mulchandani, P.; Wang, J.; Chen, W.; Mulchandani, A. *Environ. Sci. Technol.* **2005**, *39*, 8853-8857.

(23)  Lei, Y.; Mulchandani, P.; Chen, W.; Mulchandani, A. *J. Agric. Food Chem.* **2005**, *53*, 524-527.

(24)  LeJeune, K.; Wild, J.R.; Russell, A.J. *Nature.* **1998**, *395*, 27-28.

(25)  DeFrank, J.J.; Beaudry, W.T.; Cheng, T.; Harvey, S.P.; Stroup, A.N.; Szafraniec, L.L. *Chem. Bio. Interact.* **1993**, *87*, 141-148.

(26)   Asher, S.A.; Flaugh, P.L.; Washinger, G. *Spectroscopy* **1986**, *1*, 26-31.

(27)  Carlson, R.J.; Asher, S.A. *Appl. Spectrosc.* **1984**, *38*, 297-304.

(28)  Weissman, J.M.; Sunkara, H.B.; Tse, A.S.; Asher, S.A. *Science* **1996**, *274*, 959-960.

(29)  Reese, C.E.; Guerrero, C.D.; Weissmann, J.M.; Lee, K.; Asher, S.A. *J. Coll. Interface. Sci.* **2000**, *232*, 76-80.

(30)  Flaugh, P.L.; O'Donnell, S.E.; Asher, S.A. *Appl. Spectrosc.* **1984**, *38*, 847-850.

(31)  Rundquist, P.A.; Photinos, P.; Jagannathan, S.; Asher, S.A. *J. Chem. Phys.* **1989**, *91*, 4932-4941.

(32) Asher, S.A.; Holtz, J.; Liu, L.; Wu, Z.; *J. Am. Chem. Soc.* **1994**, *116*, 4997-4998.

(33) Holtz, J.H.; Asher, S.A. *Nature* **1997**, *389*, 829-832.

(34) Holtz, J.H.; Holtz, J.S.; Munro, C.H; Asher, S.A. *Anal. Chem.* **1998**, *70*, 780-791.

(35) Asher, S.A.; Holtz, J.H.; Weissman, J.M.; Pan, G. *MRS Bull.* **1998**, (October), 44-50.

(36) Sharma, A.C., Jana, T., Kesavamoorthy, R., Shi, L., Virji, M.A., Finegold, D.N., Asher, S.A. *J. Am. Chem. Soc.* **2004**, *126*, 2971-2977.

(37) Flory, P.J. *Principles of polymer Chemistry;* Cornell University Press: Ithaca, NY, **1953**.

(38) Lybradyn GS-10 OPH product specifications, Lybradyn, Inc. **2006**. Oak Brook, IL.

(39) White, B.J.; and Harmon, H.J. *Biosens. Bioelectr.* **2005**, *20*, 1977-1983.

(40) *Lange's Handbook of Chemistry,* 15th e d. Dean, J.A., Ed.; McGraw-Hill Publishers,: New York, **1999**, Chapter 8.

**CHAPTER 4:**

**Progress Towards the Development of a Point-of-Care Photonic Crystal Ammonia Sensor** - work in this chapter was a 50% effort in conjunction with Kyle W. Kimble. The primary focus of my contribution to this project was the applied sensing of ammonia in buffer and serum with the optimized PCCA material.

## 4.1 Introduction

Ammonia within bodily fluids results from the metabolic breakdown of dietary proteins, and is generated primarily in the liver, muscles, and kidneys.[1]  It is derived specifically from the deamination of the $\alpha$-amino nitrogen of amino acids and is toxic when persistent at elevated levels.  Hyperammonemia, venous blood levels of ammonia greater than 100 $\mu$M $NH_3$ in neonates, or greater than 40 $\mu$M $NH_3$ for all others, results primarily from one of four groups of diagnoses: urea cycle disorders (UCDs), organic acidemias (OAs), fatty acid oxidation defects (FAOs) and liver malfunctioning.[2,3]

Hyperammonemia results in damage to the central nervous system, including altering the transit of amino acids, water, and electrolytes across the neuronal membrane. Ammonia can also inhibit the generation of both excitatory and inhibitory postsynaptic potentials.[4,5]  The routine screening of ammonia levels should allow for treatment of at-risk patients before hyperammonemia causes retardation, neurological damage or death. The frequency of testing required to avoid the physical ramifications of hyperammonemia places a high demand on both the clinical laboratories and on the affected patients and families.[6]

Blood ammonia levels are currently determined utilizing an enzyme-based assay in which the enzyme glutamate dehydrogenase converts 2-oxoglutarate and ammonium to glutamate and water. In this reaction, the UV absorbance of the NADPH cofactor is monitored as it is converted to $NADP^+$.[2,7,8,9] This test requires sophisticated laboratory instrumentation and testing is typically done in clinical laboratories. Further complicating ammonia determinations, whole blood samples begin to generate ammonia immediately after the draw due to deamination of proteins in the red blood cells (RBCs). Blood from a healthy person can be stored at $4^o$ C for an hour, but patients with urea cycle defects must have their blood analyzed or treated within 15-30 min of the blood draw in order to obtain accurate results. This need for immediate testing presents significant obstacles for the accurate determination of ammonia and demands that the patient be tested in close proximity to the clinical laboratory.[10]

There are numerous other technologies which have been developed to detect ammonia in bodily fluids. Unlike the direct enzymatic method mentioned above, most of these are two-step processes. The first step separates ammonia from the biological matrix, and the second step is a quantitative determination. The means of separating ammonia from the blood include distillation, aeration, ion-exchange, microdiffusion, protein precipitation, or Kjeldahl extraction.[11-14] Several methods have been developed which are based on the alkaline liberation of gaseous ammonia and transport through a gas-permeable membrane. The subsequent determination of the ammonia is performed by colorimetry, titration, ion-selective electrochemistry, fluorometry, conductometry, mass

spectrometry, second-derivative spectrometry, optical waveguide spectroscopy, HPLC, or capillary isotachophoresis.[15] Several technologies have also been developed which combine liberation and quantitation into one procedure. These techniques were discussed at length in the recent review by Huizenga et al.[10]

A colorimetric approach to sensing ammonia which has been successful in solution is the Berthelot, or indophenol, reaction.[16] In this reaction, ammonia ($NH_3$) reacts with a hypochlorite ($OCl^-$) to form a monochloramine, which in turn reacts with two phenols to form an indophenol dye (Fig. 1). The concentration of $NH_3$ can be determined by monitoring the absorbance of the dye molecule at $\lambda = 640$ nm. This reaction has been extensively studied in solution for various absorbing phenolic species and hypohalite sources.[17] Various catalysts have also been explored as a means of increasing reaction kinetics. The most prevalently used catalyst is sodium nitroferricyanide (III) dihydrate (Nitroprusside, NP). Several researchers have effectively demonstrated the coupling of alkaline liberation of $NH_3$ with the Berthelot determination.[10]

The Berthelot reaction has some drawbacks. The change in the absorbance from the Berthelot reaction cannot be monitored visually because physiological concentrations of $NH_3$ result in small indophenol absorbance changes. Not only does this require the use of a spectrophotometer to measure these subtle changes, but the indophenol molecule is also subject to photodegradation. The Berthelot method is also known to suffer from interferences from other amine-containing molecules present in the analyte matrix.[18,19]
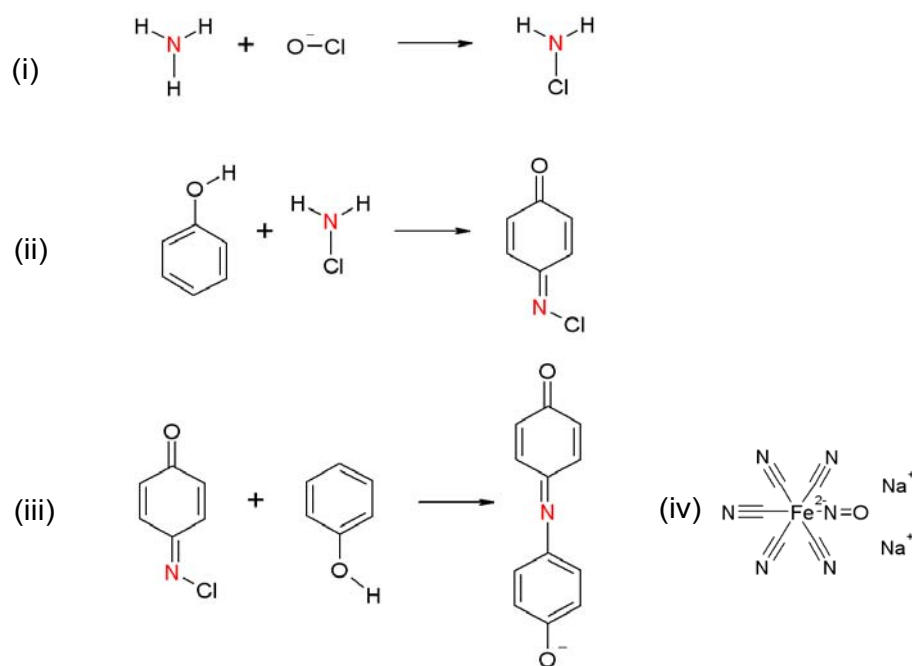
65

**Figure 1**: **The proposed reaction mechanism for the Berthelot reaction consists of three steps: (i) ammonia reacts with hypochlorite to form monochloramine at basic pH, (ii) monochloramine reacts with a phenol to form benzoquinone chlorimine, (iii) benzoquinone chlorimine reacts with a second phenol to form an indophenol. (iv) Sodium nitroferricyanide (III) dihydrate is a coupling reagent which increases the kinetics of step (ii).**

Building on the paradigm of home glucose monitoring, we seek to design a sensing material that can be incorporated into a new technology for home or bed-side point-of-care $NH_3$ monitoring. To accomplish this, the sensor must be inexpensive, reproducible, and robust. It must also be chemically sensitive, accurate, and capable of sensing very small volumes of capillary blood (20 μL). Finally, it must display information in a format that is easily interpreted.

Our $NH_3$ sensor is based on our previously developed PCCA photonic crystal sensing technology (Fig. 2).[20-33] Our PCCAs utilize an array of highly charged colloidal

particles embedded in a hydrogel matrix. The array of particles Bragg diffracts light in the visible spectral region. Our molecular recognition agent, 3-aminophenol, is covalently attached to the hydrogel. The $OCl^-$ and $NH_3$ react in the test solution to form monochloramine, which in turn reacts with two of the pendant 3-aminophenols to create a new cross-link in the hydrogel. The formation of cross-links in the hydrogel matrix increases the elastic restoring force of the hydrogel network and actuates an osmotic pressure inside the gel which causes the hydrogel to shrink in proportion to the amount of $NH_3$ present in solution. This results in a decrease in the spacing between diffracting planes of the embedded colloidal array and a blue-shift in the wavelength of light diffracted by the sensor. Our $NH_3$ sensor relies upon changes in the elastic free-energy of the hydrogel caused by the formation of cross-links. The diffraction blue-shift can be directly correlated with the amount of $NH_3$ present in the analyte solution. We have also recently improved our modeling of these PCCA sensing volume phase transitions.[34]
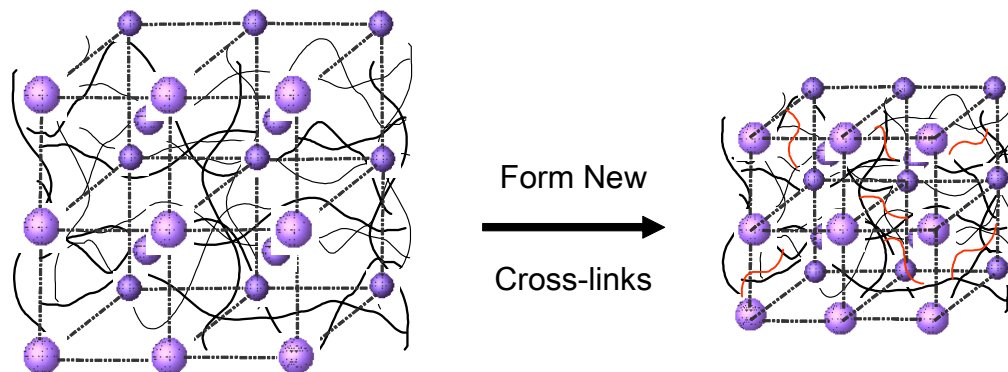


Form New

Cross-links

**Figure 2:** **The formation of indophenol cross-links results in an increase in the elastic restoring force of the hydrogel, which actuates an osmotic pressure, forcing water out of the hydrogel and thereby decreasing the volume of the gel. As a result, the spacing between diffracting planes in the PCCA decreases, and the wavelength of diffracted light blue-shifts proportional to $NH_3$ concentration.**

The wavelength of light ($\lambda_o$) diffracted follows Bragg's law: $\lambda_o = 2\,nd \sin \theta$. In our sensor, the light is diffracted by the fcc 111 plane of the embedded particle array. $\lambda_o$ depends on the plane spacing, $d$, the refractive index of the system, $n$, and the incident angle of the light, $\theta$, which is the Bragg glancing angle. Since we are sampling back-diffraction (reflectance) from light normally incident to the 111 plane of the array, $\sin \theta$ is unity.

## 4.2 Experimental

### 4.2.1 PCCA Preparation

Fig. 3 depicts the final product polymer backbone after synthesis and functionalization of the PCCA. 2-hydroxyethyl acrylate (2-HEA, 0.94 g, 8.1 mmol, Sigma), Polyethylene glycol (200) dimethacrylate (PEGDMA-200, 0.09 g, 0.25 mmol, Polysciences), glycidyl acrylate (GA, 0.04 g, 0.37 mmol, Sigma) and ethylene glycol (1.95 g, 31 mmol, J.T. Baker) were mixed and treated with $Al_2O_3$ in order to remove the inhibitor from the monomers. The mixture was centrifuged to separate the monomer from the $Al_2O_3$. 1.015 g of this solution was mixed with the colloid suspension (1.0 g, 5-10% w/w dispersion, polystyrene latex spheres, 110 nm). AG501-X8 (D) ion exchange resin ($\sim$ 0.1 g, 20-50 mesh, mixed bed, Bio-Rad) and 10 % diethoxyacetophenone (DEAP, 10 µL, 4 µmol, Aldrich) in DMSO (J.T. Baker) were mixed into the suspension in a 2-dr vial. After 15 min, the mixture was centrifuged to remove the ion-exchange resin and

was injected between two quartz discs separated by a 125- μm thick Parafilm spacer. The colloidal particles self-assemble into a crystalline colloidal array (CCA), resulting in a liquid film which diffracts light. The film was exposed to UV light (λ=365 nm) from mercury lamps (Blak Ray) for 3 hrs. A poly-HEA hydrogel network with PEGDMA cross-links forms around the CCA, resulting in a polymerized CCA (PCCA). The cell enclosing the hydrogel was opened in Nanopure water and the PCCA was allowed to equilibrate with water.



**Figure 3:** After UV polymerization and functionalization, the photonic crystal ammonia sensor contains pendant 3-aminophenols which can be cross-linked via the Berthelot reaction mechanism in the presence of ammonia and hypochlorite.

69

### 4.2.2 Attachment of 3-Aminophenol

The PCCA was placed into a 50 mM buffer solution (BBS, pH 9.2, J.T. Baker) to equilibrate before coupling. 0.5 g of 3-aminophenol (3-AMP, 4.6 mmol, Sigma) were dissolved in 10 ml DMSO (J.T. Baker) and then were diluted to 50 ml with 50 mM BBS. The solution and PCCA were placed in a 125 ml plastic container (Nalgene) and were allowed to react for ~ 8 hours. After reacting, the PCCA was rinsed every hour for 6 hours with BBS. A blank gel (hydrogel without colloid) was prepared and functionalized according to the above protocol. UV-VIS spectra of the blank gel were measured by a Varian Cary 5000 UV-VIS spectrophotometer to confirm attachment of 3-AMP by monitoring the absorbance at $\lambda = 290$ nm.

### 4.2.3 Diffraction Measurements

The diffraction of the PCCA was monitored using a fiber-optic diode spectrometer with a tungsten halogen light source (Ocean Optics) using a reflectance probe. The light is completely diffracted by the first 10-20 μm thickness of the PCCA due to the high diffraction efficiency of the embedded CCA.[24]

A PCCA (1 cm x 1cm x 125 μm) was attached to a plastic Petri dish, and was equilibrated with 5 ml of 50 mM BBS containing sodium nitroferricyanide (III) dihydrate (Nitroprusside, NP, 0.0188 g, 0.0125 M, Aldrich). A standard $NH_3$ solution was prepared by dissolving 0.03 g $NH_4Cl$ (5.6 mmol, J.T. Baker) in BBS and diluting to a total volume

of 30 ml. A NaOCl solution was prepared by diluting 2.4 ml NaOCl (5% in $H_2O$, 1.8

μmol, J.T. Baker) in BBS to a total volume of 30 ml. An initial diffraction spectrum of

the PCCA was collected, and then an aliquot of the stock $NH_3$ solution was added to each

piece of PCCA. After allowing the $NH_3$ to equilibrate for 5 min., a 28 μl aliquot of the

$OCl^-$ solution was added. The diffraction spectra were recorded at pre-selected 5 min

time intervals for a total of 120 min. The process was performed for $NH_3$ concentrations

of 30, 75, 150, and 300 μM $NH_3$, each solution contained 600 μM NaOCl. In a control

measurement, a PCCA with 3-AMP attached was exposed to 600 μM NaOCl solution

with no $NH_3$ present, and diffraction spectra were collected according to the above

protocol.


The response of a PCCA, synthesized without GA or 3-AMP, was monitored to

establish that the attached 3-AMP was responsible for the blue-shift observed. This

PCCA was tested in 0 and 300 μM $NH_3$ solutions containing 600 μM NaOCl.


The response of the PCCA to $NH_3$ was also tested in a solution which was

isotonic to physiological fluid (~ 150 mM NaCl) in order to determine whether salinity

affects the response of the sensor. The response of the sensor to concentrations of 100,

200, and 300 μM $NH_3$ was determined according to the aforementioned protocol in

solutions containing 50 mM BBS and 100 mM NaCl.

The sensor was tested in 5 ml of a 1:1 solution of BBS and male human serum from whole blood (Sigma). BBS (pH = 9.2) mixed with the serum resulted in a pH of 9.0. Four separate samples were spiked with concentrations of 30, 75, 150, and 300 μM $NH_3$. A fifth solution was not spiked, and was used in order to determine the spectral response generated from the $NH_3$ originally present in the sample. $OCl^-$ was added to the solutions after equilibration (15 min), and diffraction spectra were recorded for 120 min. These five samples were also analyzed using a Vitros Chemistry Autoanalyzer System which uses the direct enzymatic determination.[9]

The sensor was tested in 5 ml solutions of BBS and Bovine Serum Albumin (BSA, 35 mg/ml in BBS, Sigma). The response of the sensor to the addition of $OCl^-$ without $NH_3$ was determined.

## 4.3 Results and Discussion

The normal physiological range of $NH_3$ in capillary blood is 19-54 μg $NH_3$/ dL (11-32 μM $NH_3$) according to Tietz[2] or 31-122 μg $NH_3$/ dL (18-72 μM $NH_3$) according to Pesce.[3] The neurological manifestations of elevated blood $NH_3$ are expected above 250 μg $NH_3$/ dL (147 μM $NH_3$.[3] A sensor capable of determining the concentration of $NH_3$ from 10-300 μM $NH_3$ in blood would be a valuable asset to the medical community.

Fig. 4 shows the manner in which the diffraction spectrum (measured as reflectance) changes over time for 300 μM NH$_3$ in BBS.
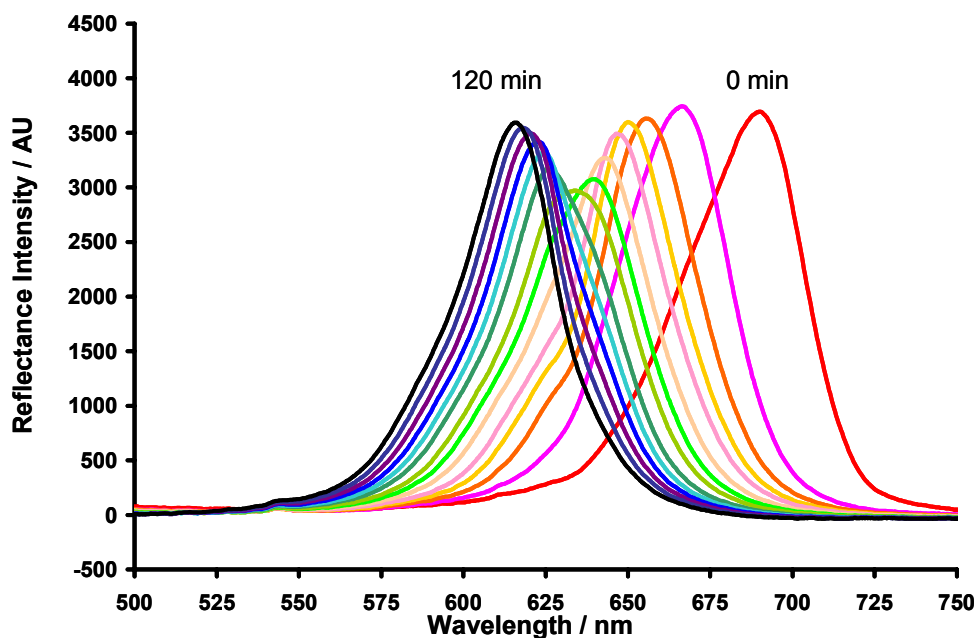


**Figure 4: Diffraction spectra of PCCA in presence of 300 μM NH$_3$. The PCCA blue-shifts continuously over the course of 120 min as NH$_3$ reacts with OCl$^-$ and 3-AMP to form an indophenol species which cross-links the hydrogel.**

The longest-wavelength diffraction peak ($\lambda_{diffraction}$ = 691 nm) corresponds to 0 min, directly after the addition of OCl$^-$. The shortest-wavelength diffraction peak ($\lambda_{diffraction}$ = 617 nm) corresponds to 120 min. The diffraction spectra shown were taken at 5 min intervals for the first 20 min and every 10 min thereafter. The sensor blue-shifts with time as the indophenol cross-links are formed. The change in the primary diffraction wavelength can be detected by a spectrometer, but it can also be observed visually.

### 4.3.1 Sensor Response to NH$_3$ in Buffer

Fig. 5 shows the diffraction blue-shift as a function of time for several concentrations of NH$_3$, as well as for a control with no NH$_3$ present. Each sample contained 600 µM OCl$^-$. The rate of blue-shift is faster for higher concentrations of NH$_3$. All samples containing NH$_3$ show diffraction blue-shifts. The control, which contains no NH$_3$, red-shifts.
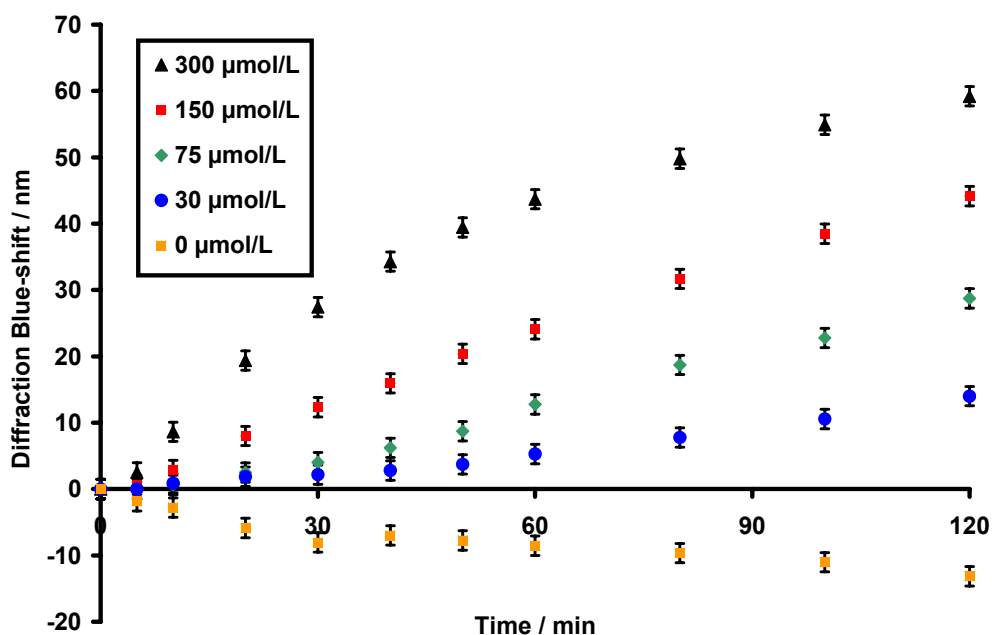


**Figure 5: Diffraction blue-shift versus time for ammonia-sensing PCCA in BBS at pH 9.2 containing 600 µM OCl$^-$. The sensor displays distinctly different rates of diffraction shift for differing NH$_3$ concentrations; the control, containing no NH$_3$, actually red-shifts. The error bars are the average over the different time measurements of the standard deviation between replicate trials ($\lambda_{\text{diffraction}} = \pm 1.46$ nm, N = 3). The relative standard deviation remained fairly constant over time.**

The lack of blue-shift in the control indicates that no cross-links are formed without $NH_3$ present. The diffraction red-shift is presumably caused by the hydrolysis of the poly-ethylene glycol cross-links esters at basic pH; this decreases the elastic restoring force of the PCCA and causes the hydrogel to expand. Since the red-shift is accelerated in the presence of $OCl^-$, we presume the $OCl^-$ accelerates the hydrolysis of the cross-link esters. Our hypothesis that the cross-link ester groups are being hydrolyzed is confirmed by observing an un-functionalized PCCA (no GA or 3-AMP) swell upon addition of $OCl^-$. The extent and rate of red-shift was independent of the presence of 3-AMP. Fig. 6 shows the $NH_3$ response calibration curves constructed from the observed shifts at 60 and 120 min in 50 mM BBS. The curve has been corrected by subtracting the red-shift of the control from each spiked sample.
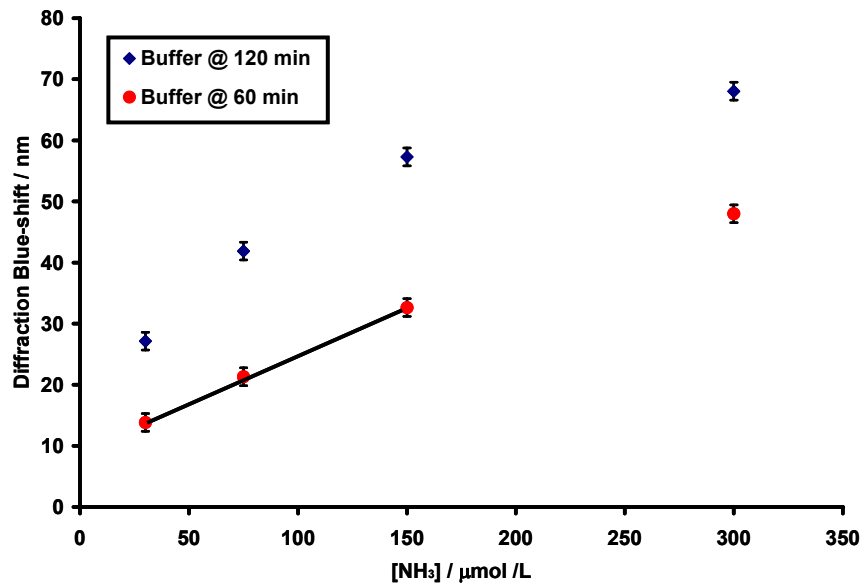


**Figure 6: Calibration curve based on the response of our sensor to $NH_3$ in BBS (pH=9.2) containing 600 $\mu$M $OCl^-$ at 60 and 120 min. This sensor shows a linear response between 30 and 150 $\mu$M $NH_3$ at 60 min.**

The response of the sensor is linear at 60 min for $NH_3$ concentrations between 30 and 150 μM, but begins to saturate at $NH_3$ concentrations greater than 150 μM. The response is curvelinear at longer times. The deviation from linearity presumably occurs because the concentrations of available $OCl^-$ and 3-AMP are depleted as the reaction proceeds. This effect is exacerbated at longer time intervals and higher $NH_3$ concentrations. At low concentrations of $NH_3$, the 3-AMP and $OCl^-$ concentrations are present in sufficient excess such that the rate depends mainly on the concentration of $NH_3$. Harfmann and Crouch previously established that the Berthelot reaction is first order with respect to the $NH_3$ when the $OCl^-$ and phenol are in excess.[35] The linear region of the 60 min calibration was used to calculate a detection limit. This limit was found to be 27 μM $NH_3$ at a signal to noise ratio of 3/1.

We examined the dependence of response on ionic strength. We utilized samples which were isotonic with serum and which had a salt concentration of 150 mM NaCl. The rate and response was indistinguishable from the behavior of our sensor in 50 mM BBS. These results confirm that the sensing mechanism is not affected by high ionic strength and that the volume change is essentially independent of the ionic free energy of the system.

## 4.3.2 Sensor Response to $NH_3$ in Serum

We also examined the response of our sensor to samples in diluted human blood serum. The serum presents a more complex sensing medium than BBS due to the presence of salts, amino acids, and proteins. Although we seek to develop a sensor which works in whole blood, we are first testing our sensor in serum to avoid the errors associated with the generation of $NH_3$ in stored whole blood.[10] RBCs contain enzymes that can increase the concentration of $NH_3$ with time after the blood is drawn. This rapidly raises the level of $NH_3$ in the samples to hyper-physiological levels.

Fig. 7 displays the diffraction blue-shift as a function of time for four spiked serum samples (30, 75, 150, 300 µM $NH_3$ spikes) as well as the normal, unspiked, sample.
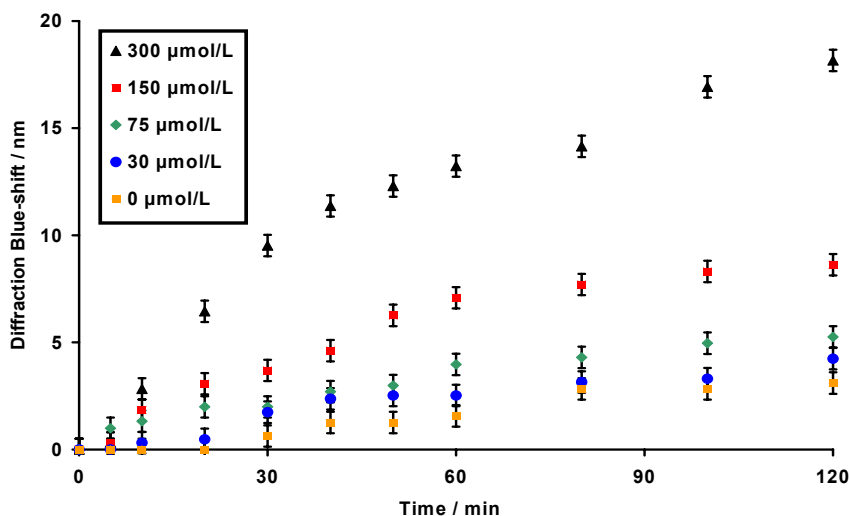


**Figure 7: We measured the PCCA response of four spiked serum samples and an un-spiked sample. All samples contained 600 µM OCl⁻ and had a pH of 9. We found the serum contains $NH_3$ on the order of the physiological concentration for healthy adults. The error bars are the average of the standard deviation between replicate trials ($\lambda_{diffraction} = \pm 0.57$ nm, N = 3).**

Unlike the buffer, normal human serum contains a background level of $NH_3$. To determine the concentration of $NH_3$ in our unspiked sample, we used a Vitros 950 Chemistry System, the clinical instrument utilized by the University of Pittsburgh Medical Center. According to the Vitros determination, our normal serum solution had a background concentration of 4 µM $NH_3$.

The most remarkable difference between the sensor in buffer and in serum is the response to low $NH_3$ concentrations. In buffer without $NH_3$, the sensor responds to the addition of $OCl^-$ by red-shifting $\Delta\lambda = 14$ nm. In the normal serum solution containing only 4 µM $NH_3$, the sensor responds to the addition of $OCl^-$ by blue-shifting $\Delta\lambda = 3$ nm. We established that proteins were responsible for the blue-shift by analyzing an ammonia-free protein-rich solution of BSA (70 mg BSA/ml in BBS). The sensor also responded with a slight blue-shift ($\Delta\lambda = 3$ nm) in the two hours following the $OCl^-$ addition. We conclude the proteins in the serum are primarily responsible for the blue-shift in the unspiked serum.

Our observations correlate well with the Hawkins et al.[36,37] description of the reactivity of $OCl^-$ towards proteins. They showed that $OCl^-$ modifies the amino-acid side-chains without significant degradation to the protein backbone at low $OCl^-$ concentrations. Interactions of this type would result in a reduction of the available $OCl^-$

which would reduce the kinetics and extent of the reaction between OCl$^-$ and NH$_3$. While slow compared to the reaction with NH$_3$, the products of reactions between OCl$^-$ and serum proteins could react further with the 3-AMP species on the hydrogel to cause the slight blue-shift observed.

The diminished response observed in serum can be explained by previous studies, which report that the Berthelot reaction is subject to interference from proteins.[18] Ngo et al.[19] found that a solution containing 0.1% human serum caused an interference of 4%. The manifestations of this interference are obvious in our sensor as the response rate and the spectral window are both decreased by a factor of three in 50% human serum solution. Despite the interference, we were able to establish a calibration curve for the spectral shift in response to the NH$_3$ concentration in serum. Fig. 8 shows the calibration curve of the sensor's response to NH$_3$ at 60 min.
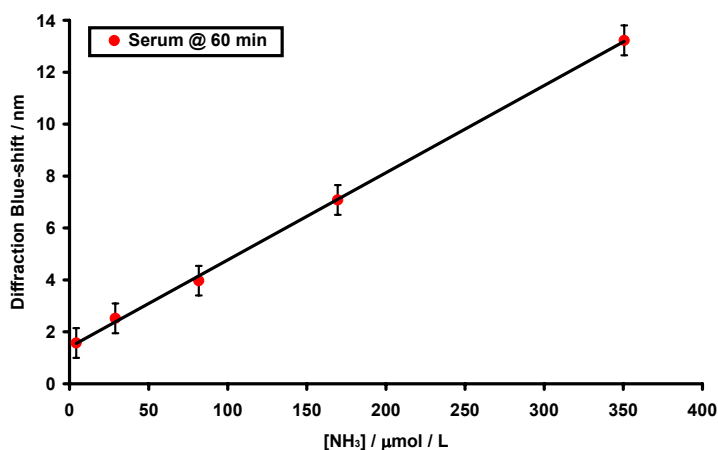


**Figure 8**: **Calibration curve for the response of our sensor to NH$_3$ in a 1:1 solution of serum and BBS at 60 min. Concentrations of NH$_3$ were determined using the Vitros Autoanalyzer. Error bars are equal to the standard deviation ($\lambda_{diffraction} = \pm 0.57$ nm, N = 3).**

79

The response of the sensor is linear for concentrations of $NH_3$ between $0 - 350$ $\mu M$. We determined that the detection limit for our sensor was 50 $\mu M$ $NH_3$ at 60 min, and increases to 60 $\mu M$ $NH_3$ at 120 min. The detection limit was determined from three times the standard deviation of our control ($\lambda = 0.57$ nm). The detection limit for the observed blue-shift ($\lambda = 3.12$ nm) was used to calculate the $NH_3$ detection limit utilizing the linear regression. The increase in detection limit with time is due to the increase in the standard deviation of our spectral shifts at longer times and higher concentrations. The detection limit would also be increased at smaller times as the slope of the response versus concentration increases over time. The $NH_3$ present in the unspiked serum is below the detection limit of our sensor and cannot be distinguished from a serum sample containing no $NH_3$. Furthermore, the 30 $\mu M$ spiked sample cannot be distinguished from the unspiked sample at the >99% confidence level. Table 1 compares our sensor with current standards in clinical $NH_3$ sensing.

**Table 1: Comparison of clinical reference interval with PCCA and Vitros $NH_3$ methods**

| Clinical Reference Interval | 10 - 300 $\mu M$ $NH_3$ |
|---|---|
| Ammonia Sensitive PCCA | 50 – 350 $\mu M$ $NH_3$ |
| Vitros 950 Chemistry Analyzer | 1.0 – 500 $\mu M$ $NH_3$ |

## 4.4 Conclusions

In the work described here, we devised an $NH_3$ sensitive material in which we utilize the Berthelot reaction in our Polymerized Crystalline Colloidal Array (PCCA)

sensing platform. Our material has the capability to quantitatively determine $NH_3$ concentrations between 50 and 350 µM $NH_3$ in human blood serum which brackets the clinically relevant interval. The material responds to 300 µM $NH_3$ additions with a spectral blue-shift of $\Delta\lambda = 60$ nm in BBS and $\Delta\lambda = 20$ nm in serum solution at 120 min. The detection limit is 27 µM $NH_3$ in BBS at 60 min and 50 µM $NH_3$ in 50% serum solution at 60 min with a confidence level of >99%.

### 4.4.1 Future Work and Outlook

We are currently optimizing our reaction conditions, sample preparation, and hydrogel composition to improve sensitivity, spectral shift, and response time. We anticipate that our technology could be engineered to combine separation and detection into a single system through modification of the diffusion characteristics of our hydrogel or by utilizing our material's thin film morphology, which could be incorporated into a more complex sensing device. Separation of $NH_3$ from the sample would prevent interferences (RBCs, proteins, clotting, etc.) from affecting the sensor's performance.

The goal of our optimization is to develop a sensor responsive to $NH_3$ concentrations over the clinically relevant interval with distinct visual color changes. Our sensor could then be used as a point-of-care device for the detection of blood $NH_3$ concentrations to monitor conditions deriving from urea cycle disorders, organic acidemias, fatty acid oxidation defects, and hepatic disorders in order to prevent patients from reaching hyperammonemic states. The ability to monitor these conditions at the

bedside or at home with an inexpensive, robust system would provide long-term benefits to both patients and health care providers.

### 4.4.2 Acknowledgments

## 4.5 References

(1) Huizenga, J.R.; Gips, C.H.; Tangerman, A. *Ann. Clin. Biochem.* **1996***, 33, 23.

(2) Tietz, N.W. *Clinical Laboratory Guide to Laboratory Tests, 3ʳᵈ Ed.* **1995,** WB Saunders, Philadelphia.

(3) Pesce, A.J.; and Kaplan, L.A. *Methods in Clinical Chemistry,* **1987,** CV Mosby Company, St. Louis, MO.

(4) Hazell, A.S.; and Butterworth, R.F. Exp. Biol. and Med. 1999, *222*, 99.

(5) Campion, M. *Blood Ammonia: a critical measurement,* **2003**, in BIMDG Bulletin Spring 13.

(6) Bachmann, C. *Eur. J. Pediatr.* **2003**, *162,* S29.

(7) Mondzac, A.; Ehrlich, G.E.; and Seegmiller, J.E. *J. Lab. Clin. Med.* **1965**, *66,* 526.

(8) Van Anken, H.C.; Schiphorst, M.E. *A. Clin. Chim. Acta.* **1974**, *56,*151.

(9) Bostian, K.A., and Betts, G.F. *Biochem. Journal* **1978**, *173,* 773.

(10) Huizenga, J.R.; Tangerman, A.; Gips, C.H. *Ann. Clin. Biochem.***1994**, *31, 529.*

(11) Mann, L.T. *Anal. Chem*. **1963**, *35*, 2179.

(12) Reay, P.F. *Anal. Chim. Acta.* **1985**, *176*, 275.

(13) Lau, K.T.; Edwards, S.; and Diamond, D. *Sens. Actuators B*. **2004**, *98,* 12.

(14) Daridon et al. *Sens. Actuators B*. **2001**, *76,* 235.

(15) Zellmer, S.; Katenborn, G.; Rothe, U.; Lehnich, H.; Lasch, J.; and Pauer, H.D. *Anal. Biochem.* **1999**, *273*, 163.

(16) Berthelot, M. Repert. Chim. Appl. **1859**, *1*, 284.

(17) Searle, P.L. *Analyst,* **1984**, *109*, 549.

(18) Gips, C.H.; and Reitsma, A. *Clin. Chim. Acta* **1971**, *33*, 257.

(19) Ngo, T.T.; Phan, A.P.H.; Yam, C.F. and Lenhoff, H.M. *Anal. Chem.* **1982**, *54*, 46.

(20) Krieger, I.M.; and O'Neill, F.M. *J. Am. Chem. Soc.* **1968**, *90*, 3114.

(21) Hiltner, P.A.; and Krieger, I.M. *J. Phys. Chem.* **1969**, *73*, 2386.

(22) Hiltner, P.A.; Papir, Y.S.; and Krieger, I.M. *J. Phys. Chem.* **1971**, *75*, 1881.

(23) Carlson, R.J.; and Asher, S.A. *Appl. Spec.* **1984**, *38*, 297.

(24) Runquist, P.A.; Photinos, P.; Jagannathan, S.; and Asher, S.A. *J. Chem. Phys.* **1989**, *91*, 4932.

(25) Asher, S.A.; Holtz, J.H.; Liu, L.; and Wu, Z. *J. Am. Chem. Soc.* **1994**, *116*, 4997.

(26) Weissman, J.M.; Sunkara, H.B. Tse, A.S.; and Asher, S.A. *Science,* **1996**, *274*, 959.

(27)  Ito, K.;  Nakamura, H.; and  Ise, N. *J. Chem. Phys.* **1986**, *85*, 6136.

(28)  Monovoukas, Y.; and Gast, A.P.  *J. Colloid Interface Sci.* **1989**, *128*, 533.

(29)  Okubo, T. *Acc. Chem. Res.* **1988**, *21*, 281.

(30)  Asher, S.A. U.S. Patents 4,627,689 (**1986**), 4,632,517 (**1986**), 5,281,370 (**1994**), 5,452,123 (**1995**).

(31)  Holtz, J.H.; and Asher, S.A. *Nature* **1997**, *389*, 829.

(32)  Holtz, J.H.; Holtz, J.S.; Munro, C.; and Asher, S.A. *Anal. Chem*. **1998**, *70,* 780.

(33)  Pan, G.; Kesavamoorthy, R.; and Asher, S.A. *J. Am. Chem. Soc.* **1998**, *120,* 6525.

(34)  Goponenko, A.V.; and Asher, S.A. *J. Am. Chem. Soc*. **2005**, *127, 10753.*

(35)  Harfmann, R.G.; and Crouch, S.R. *Talanta.* **1989**, *36*, 221.

(36)  Davies, M.J. *Biochim. Biophys. Acta.* **2005**,  *93,* 1703.

(37)  Hawkins, C.L.; Pattison, D.I.; and Davies, M.J. *Amino Acids* **2003**, *25*, 259.

# CHAPTER 5: SUMMARY AND FUTURE WORK

## 5.1 Summary of Work

We developed novel sensors for several important environmental and clinical analytes. Each sensor relies upon the manipulation of one of the Gibbs free energy parameters which affect the hydrogels' response to their environment. Each of these free energy changes results from the presence of an analyte in solution, which generates a change in the hydrogel volume that shifts the wavelength of light Bragg diffracted by the embedded CCA. Two of these sensors utilize sensing motifs which rely upon enzymes as recognition agents for analyte detection. We have chosen important analytes which have been focal points of recent research in both the medical and environmental sensing fields.

Chapters 2 and 3 discuss the development of two organophosphate nerve agent sensors. Organophosphates are produced industrially on a very large scale as agricultural pesticides. These pesticide species, which consist of parathion, methyl-paraoxon, and paraoxon, have variable half-lives and can persist in the environment for weeks. As a result, they pose significant threats to groundwater and drinking water sources. Furthermore, OPs also include the chemical warfare agents sarin, soman, and VX gas. These potent OPs inhibit the central nervous system and can cause paralysis and death at very low levels of exposure. There currently exists a significant threat of chemical warfare, and the military requires an inexpensive, reliable sensor for detection of OP species both in drinking water supplies and in the environment.

In Chapter 2, we demonstrated the development and application of a PCCA sensing material functionalized with the acetylcholinesterase (AChE) enzyme which operates as a dosimeter due to irreversible binding of the OP to the AChE's catalytic serine residue. We demonstrated that the response mechanism involves the creation of an anionic phosphonyl-enzyme species which results from the OP inhibition. In low-ionic strength solution, the anionic phosphonyl-enzyme species creates a Donnan potential which causes the hydrogel to swell in proportion to the amount of OP bound. The AChE-based OP sensor displays femtomolar detection limits which are currently about one million fold lower than the detection limits of other current of sensors. The AChE-based OP sensor is capable of detecting parathion and could potentially be used for ultra-trace detection of OP species in pure aqueous environments, such as the military's tactical online water purification systems.

The OP sensor presented in Chapter 3 is an organophosphorus hydrolase-based OP sensor. The recognition event decreases the local pH inside the gel, which decreases the free energy of mixing of the PCCA. The free energy decrease causes the PCCA to shrink, which blue-shifts the wavelength of Bragg-diffracted light. The OPH-based OP sensor offers several advantages over the AChE-based OP sensing system. The sensor is reversible, and can be rinsed, stored and reused, which cuts the costs associated with production and storage of sensors. The sensor operates in real time to sense changing OP concentrations. The sensor also functions in high ionic strength solutions, and can be utilized in any aqueous sensing medium with minimal sample preparation.

Chapter 4 details the development of a sensor for clinical ammonia, whose presence in physiological fluids is indicative of a host of physical maladies ranging from liver and renal malfunction to inborn amino acid metabolic deficiencies. Development of an easy-to-use, inexpensive sensor for monitoring ammonia levels in physiological fluids would greatly improve point-of-care treatment for patients afflicted with such diseases, especially in third world countries which lack the means to obtain or deploy current diagnostic technologies.

We developed a PCCA material which senses ammonia via creation of cross-links. The sensor utilizes the Berthelot reaction, in which ammonia and hypochlorite form a monochloramine species which covalently links two pendant phenol species to form an indophenol cross-link. Cross-link formation increases the elastic restoring force of the hydrogel and blue-shifts the wavelength of Bragg-diffracted light. The sensor detects ammonia over much of the clinical reference interval, covering the range of $50 - 350$ μM $NH_3$ in human serum. The sensor shows promise as a point-of-care sensing device which could allow physicians to perform qualitative analysis of serum, plasma, urine, etc. in order to aid diagnosis of disease states. The sensor could also potentially be coupled with enzymatic reactions which catalyze amino acids to produce ammonia in order to detect concentrations of specific amino acids, permitting diagnosis of amino acid metabolism diseases. The limitation of the current sensor is its small spectral window and the diminished spectral response which is observed in serum due to inhibition of the Berthlelot reaction. This inhibition results from the reaction of the hypochlorite with serum protein amine groups, which diminishes the availability of the hypochlorite to form the monochloramine species.

## 5.2 Future Work

We demonstrated the development and application of several novel photonic crystal sensing materials for detection of organophosphate species and ammonia in bodily fluids. These sensors provide robust responses to their analytes; each sensor responds via a change in a separate free energy parameter. In the following, we will suggest methods for optimization of the sensors' mechanical properties, functional group concentrations, and sample solution changes which should result in either faster response times, decreased limits of detection, or increased spectral response windows which span the entire visible region of the electromagnetic spectrum. The goal of the optimization is to produce sensors which are capable of direct analyte detection and quantification according to the diffracted color. Also, since changes in diffraction can sometimes be imperceptible to the naked eye, the sensors could be utilized with a small spectrometer which measures the diffraction using a small handheld spectrophotometer. The device could then translate the diffraction wavelength into an analyte concentration which would then be displayed on a palm-pilot type electronic device.

In Chapter 2 we described the development of a novel AChE-based OP sensor which operates as a dosimeter. Each molecule of AChE attached to the PCCA binds one molecule of OP. Because the binding is irreversible, once all the AChE binds OP the sensor is saturated. We previously considered the quantity of OP present in samples which contained substoichiometric ratios of OP to AChE only after the spectral response had reached an endpoint. However, the sensor is capable of quantitative analysis of samples containing both substoichiometric and greater than stoichiometric OP levels.

Figure 1 illustrates the response to OP levels which are both above and below

stoichiometry with the amount of AChE attached to the sensor.
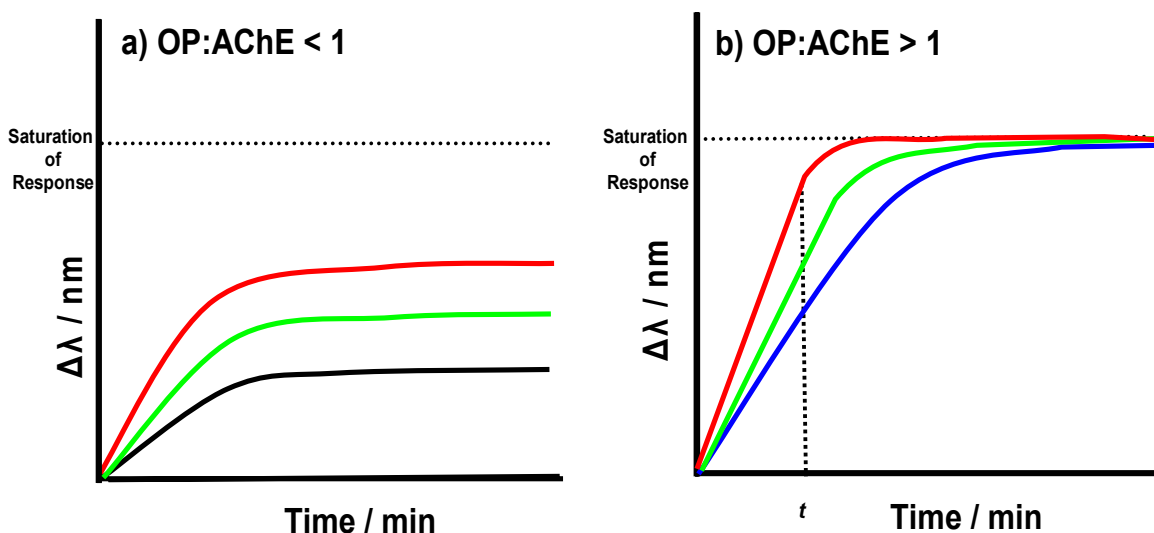


**Figure 1: a) displays the spectral response as a function of time for three different OP solutions which contain OP levels below stoichiometry with the AChE attached to the sensor. The number of OP moles present increases from black to green to red. The amount of OP can be quantified according to the final equilibrium spectral shift of the sensor. b) displays the spectral response of the sensor to OP concentrations which are above stoichiometry with the AChE. The amount of OP present increases from blue to green to red. If the sensing volume is held constant, a solution containing more OP will saturate the diffraction faster. By selecting a point in time, $t$, which occurs prior to saturation, the spectral shift can be correlated to the amount of OP in the solution.**

OP levels below stoichiometry can be quantified by allowing the sensor to achieve

equilibrium swelling (Fig. 1a), and the extent of diffraction shift directly correlates to the

amount of OP in the sample. Above stoichiometric ratios, equilibrium swelling

diffraction cannot be correlated with the amount of OP present because the responses all

reach the same saturation of spectral response (Fig. 1b). In order to quantify the amount

of OP in the sample, a point $t$ in time must be selected at which the rate of response can

be compared for OP levels above stoichiometry. Using this approach, samples containing more OP will display faster response rates. Therefore, reading the response at time $t$ will allow the quantification of OP levels which are greater than stoichiometric with AChE.

When preparing the AChE-based OP sensor, we utilized the same acrylamide/bisacrylamide hydrogel composition which previously allowed swelling responses that covered a 200 nm total spectral window in our low ionic strength glucose sensor.[1] Thus, we believe that our polymer network is capable of considerable swelling. We can expand our spectral window by attaching more AChE to the hydrogel backbone, which will increase the saturation response level. However, increased AChE attachment will not affect the response rate because it is limited by the rate of OP diffusion.

There are three essential strategies for increasing the enzyme loading. The first strategy is to increase the incubation time of the PCCA in AChE, which would allow time for more of the enzyme to diffuse into the hydrogel. Clearly, we are able to successfully diffuse and covalently attach a small amount of AChE inside the hydrogel, we calculated about $3.9 \times 10^{-12}$ moles of AChE attached using Ellman's acetylthiocholine assay. This correlates well with the amount of OP which saturates the response of the hydrogel ($4.3 \times 10^{-12}$ moles). We attempted to increase the loading of AChE by increasing the pre-coupling incubation time of the sensor in AChE solution from 1 to 3 days. However, when we quantified the amount of functional AChE attached to the PCCA, we found no increase in the maximum velocity of substrate turnover, which indicated that there was not a significant increase in the amount of AChE attached to our sensor. Furthermore, the spectral response window was not increased. Also, extensive post-coupling rinsing

90

studies indicated that washing the PCCA for several days removed about 90% of the AChE. We are still uncertain whether this result is due to poor diffusion of the enzyme or inefficient coupling chemistry. Clearly, only a small amount of AChE is attached to the polymer network as proven by both the Ellman's assay and the OP saturation response calculations. In the likelihood that the problem is related to the steric restrictions which hinder AChE diffusion, we will make physical changes which will increase the hydrogel's porosity in order to diffuse and attach more AChE into our PCCA.

The second strategy for attaching more AChE is to develop more porous hydrogels which will permit more of the large AChE enzyme (~260 kDa) to diffuse into the PCCA. Hydrogel porosity can be increased by cutting the overall percentage of acrylamide polymer, which will result in less polymer entanglement and greater equilibrium swelling.[2,3] We can also add nonreactive monomers during polymerization which have high molecular weights, such as a large poly(ethyleneglycol) with a molecular weight of 20-80 kDa, which would act as fillers and could be rinsed out of the PCCA after polymerization. Use of such large molecular weight unreactive monomers is a frequently utilized technique for increasing hydrogel porosity.[4,5]

The third approach for increasing AChE attachment would be to dissociate the tetrameric native AChE enzyme, which is a very large molecule (260 kDa) into much smaller monomeric units (~ 65 kDa). The monomeric AChE will be able to diffuse into the hydrogel more freely. However, literature suggests that certain techniques for dissociating cholinesterases may decrease the activity of the catalytic units by lowering the substrate turnover.[6,7] However, several studies [8,9] have shown that OP binding to the

site is less affected by denaturation than substrate turnover due to the significantly higher affinity constants of AChE for OPs ($K_a \sim 10^{12}$ L/mol for OPs vs. $K_a \sim 10^7$ L/mol for acetylcholine).[8-12] We will need to perform experiments to assess the degree of AChE activity loss associated with the dissociation of the native enzyme to its monomeric units; loss of activity may not significantly affect OP binding capability.[6,7]

We will study whether these optimizations enable increased AChE loading by performing UV-VIS absorption measurements on blank hydrogels before and after AChE coupling. Attachment of more AChE will result in a larger spectral response window due to an increase in the saturation response level.

The AChE-based OP sensor can also be optimized to cover the entire visible spectrum (400 – 750 nm) by decreasing the hydrogel cross-link density. We will decrease the concentration of bisacrylamide added to the initial polymerization mixture. The decreased cross-link density will permit the sensor to swell more in response to the Donnan potential created when AChE binds OPs. Thus, a larger diffraction red-shift will occur when compared to the response achieved by the current sensor in the same OP concentrations. Reduction of the cross-link density will allow the sensing response to cover the entire visible light spectrum.

Practical application of the AChE-based OP sensor is limited by the variable ionic strength of real samples, which will swamp out the Donnan potential and prevent sensing. For example, Lee and Asher reported reduction in the swelling of a carboxylated PCCA by NaCl concentrations as low as 0.1 mM NaCl.[13] Furthermore, Donnan potential

swelling was completely swamped out by a concentration of 10 mM NaCl. Also, other inhibiting species such as carbamates can be present which will inhibit OP binding. It does appear that the AChE-based OP sensor shows significant potential for use by the military for monitoring its mobile ultrapure water systems for OP breakthrough. The low detection limit would provide notification of OP breakthrough at much lower OP levels, and perhaps faster, than other current OP sensing technologies.

The limitations of the environments in which the AChE-based OP sensor can be practically applied led us to develop a new OP sensing material which operated via a different sensing mechanism. In Chapter 3 we demonstrated a bimodular OP sensor which relies upon OPH catalyzed hydrolysis of OPs to produce protons. These protons lower the interior pH of the hydrogel and titrate pendant phenolates, lowering the hydrogel's free energy of mixing and blue-shifting the diffraction. The sensor can be optimized to improve the spectral response window through modification of the sensor's polymer backbone composition. Optimization of the current OPH sensor should provide a sensing material which can detect lower levels of OPs than our current sensor in environmental samples on the order of a few minutes. This sensor could be quite useful for sensing OPs in contaminated environmental samples. It could be incorporated into a real-time sensing device with a spectrophotometric readout for utilization in the field by military personnel.

We will improve the spectral window of the sensor by switching to a polyacrylamide or poly(vinyl alcohol) polymer backbone. Our current sensor consists of a 17% (w/v) poly(2-hydroxyethylacrylate) network. Lowering the polymer percentage of

this sensing material is impossible because microsyneresis processes occur at lower concentrations during polymerization. Microsyneresis is the phase separation of a polymer from the solvent which occurs due to the hydrophobicity of the growing polymer chain. This results in a dispersion of polymer microdomains within the hydrogel.[15] This results in poorly-diffracting PCCAs because the hydrophobic microdomains of polymer destroy the diffraction from the PCCA presumably due to the combined effects of diffuse scattering of visible light by the polymer particles[15] as well as the physical disordering of the colloidal particles by the poly(2-HEA) particles. [15-17] Switching to a more hydrophilic polymer will allow us to lower the polymer percentage and avoid microsyneresis because the hydrogel's increased solubility will permit more swelling in aqueous media during polymerization.

We attempted to increase the spectral response window of the sensor by decreasing the cross-link density. Experiments in which the concentration of the PEGDMA-200 cross-linker was decreased in our current sensing material showed no increase in the spectral response window of the sensor. We hypothesize that this is because the 17 % poly(2-hydroxyethylacrylate) hydrogel we developed is too highly-intertangled  to permit significant swelling. Switching to an acrylamide polymer network will allow us to decrease the polymer percentage, and to subsequently increase the response spectral window by decreasing the concentration of bisacrylamide cross-linker, which will allow the hydrogel to swell more. OPH sensors with fewer cross-links will initially be more swollen than our present sensor; protonation of the pendant phenolates will result in a more significant degree of shrinkage of the PCCA.

We can also attempt to avoid the microsyneresis effect by using solvents which will keep the growing polymer chain soluble during polymerization. Other members of our group found experimentally that preparation of a similar hydrogel system based on poly(2-hydroxyethyl)methacrylate (HEMA) using diethylene glycol as a cosolvent enabled reduction of the hydrogel polymer content without the onset of microsyneresis during photopolymerization.

In Chapter 4 we presented an ammonia-sensitive PCCA material which detects serum $NH_3$ with a linear detection range between $50 - 350$ $\mu M$ $NH_3$. The sensor works via the Berthelot reaction, in which ammonia and hypochlorite form monochloramine at pH 8-10, which subsequently cross-links two pendant phenol moieties attached to the sensor backbone. Formation of additional cross-links causes an increase in the elastic restoring force of the polymer network which causes the hydrogel to shrink, which decreases the lattice spacing of the embedded CCA and blue-shifts the diffracted wavelength. The sensor can be optimized to operate over the entire visible spectral region via changes in the composition of the polymer backbone of the hydrogel.

The ammonia sensor can be optimized in several different ways in order to improve the spectral response window. We utilized a poly(2-hydroxyethylacrylate) polymer system similar to the one used for the OPH-based OP sensor. This backbone was utilized because it provided an amine-free polymer system, which reduces cross-reactivity of the polymer backbone with hypochlorite. However, the ability to lower the polymer percentage and cross-link density of this particular system is severely limited due to the previously explained microsyneresis phenomenon which occurs during

polymerization at decreased polymer concentrations. As discussed previously for optimization of the OPH sensor, we may be able to reduce the polymer content and avoid microsyneresis by utilizing diethylene glycol as a cosolvent during polymerization.

Our group is currently focusing on the development and optimization of other amine-free polymer systems which will provide a more robust response to ammonia by enabling polymer concentrations which give rise to improved mechanical network properties. We can utilize a poly(vinylalcohol, PVA) polymer backbone system. This system will still lack amine groups and thus have a low degree of reactivity with hypochlorite, however it will also provide a more hydrophilic network which will be more swollen than poly(2-hydroxyethylacrylate) in aqueous solution. Furthermore, the new PVA backbone will provide the ability to significantly reduce the polymer percentage (from 17% to 5-10%). This will provide a less-entangled polymer network whose cross-link density can be reduced to expand the spectral response window. PVA is an ideal polymer system for a biological fluid sensing device. PVA is highly biocompatible because its fully hydrolyzed chemical backbone prevents adhesion of proteins, which makes it an excellent coating material for implantable devices such as stents.[18] PVA also displays very low toxicity and immunogenicity, and is not degraded by the body.[18-23] The material's stability makes it ideal for *ex situ* sensing of biological fluids as well as for *in vivo* applications due to its low degree of reactivity with tissue and biological media.

Improvement of the ammonia sensor's spectral response and sensitivity may also be obtained through optimization of the analyte solution. Optimization of the catalyst

concentration could lead to improved response times. Once we replace the hydrogel network, we will re-optimize the NP catalyst concentration and explore the use of other catalyst molecules to improve the rate of response. We previously found that the optimal concentration of nitroprusside (NP) which lead to the largest response was 12.5 mM NP. We will re-optimize the solution to determine whether this is still the case. Berthelot reaction literature suggests that the NP provides the highest reaction rate among catalyst molecules, however at low ammonia levels excessive NP catalyst concentrations can result in light-induced breakdown of the NP molecule.[24] Some studies suggest that an alternative catalyst, sulfitopentacyanoferrate (SpF), is a more stable catalyst which is not subject to the same degree of photodegradation as NP.[25]

The ammonia sensor also suffers from limitations imposed by the cross-reactivity of the hypochlorite species with protein amine groups, which interferes with formation of the monochloramine.[24,26] The reduced spectral response in serum may additionally be attributed to physical adsorption of proteins to the hydrogel backbone which reduces the effective spectral window. Sharma et. al. found that serum contains proteins which diffuse into their creatinine sensing IPCCA and blue-shifted the diffraction wavelength during the pre-equilibration period.[27] To limit this adsorption effect, we will integrate filtration materials which will separate the PCCA sensing material from the analyte solution and limit the diffusion of proteins into the PCCA. Development of such a material would limit the reduction in spectral window which arises from the physical adsorption of proteins into the PCCA. This would also prevent local competition between proteins and ammonia inside the hydrogel for hypochlorite. By preventing protein contact

with the sensor, the filtration material should limit the hydrogel shrinkage which occurs due to protein adsorption to the PCCA.

Finally, we will examine the efficiency of sensing in plasma versus sensing in serum. We believe that plasma provides more interfering species but less endogenous ammonia than serum matrices. Plasma is prepared by adding heparin, which prevents coagulation of the blood. The sensor would be immediately placed in the plasma sample after heparinization. Serum, however, is produced by allowing the blood to clot for about 20 minutes, removing the clot and then centrifuging to obtain the supernatant. Serum contains fewer proteins, which could lower the degree of interference with the hypochlorite. However, red blood cells begin to produce ammonia immediately upon removal from the body, and more ammonia could be produced due to the requisite time length of serum preparation.

Optimization of the sensing conditions as well as the physical parameters of the hydrogel should result in a robust ammonia-sensitive PCCA material which will be capable of detecting ammonia within the clinically relevant interval (1-300 μM) on the order of a few minutes. Development of such a simple-to-use, cost-effective material would revolutionize point-of-care disease diagnosis and detection for both home monitoring as well use in third world countries.

Looking beyond simple direct ammonia detection, we also envision utilization of the sensor in conjunction with a separate "dipstick" with an ammonia producing enzyme immobilized inside a thin polymer film or foam constructed from poly(vinyl alcohol) or

from polyurethane. Several enzymes are available which metabolize amino acids and produce ammonia. The dipstick could be immersed into the analyte solution and catalyze the amino acid analyte of interest. The solution would subsequently be exposed to the ammonia sensor to analyze the concentration of amino acid present in the sample. This would even further extend the capabilities of point-of-care sensing.

## 5.3  References

(1)   Asher, S.A.; Alexeev, V.L.; Goponenko, A.V.; Sharma, A.C.; Lednev, I.K.; Wilcox, C.S.; and Finegold, D.N. *J. Am. Chem. Soc.* **2003**, *125*, 3322-3329.

(2)   Wu, S.; Li, H.; and Chen, J.P. *J. Macromol. Sci.C.* **2004**, *44*, 113-130.

(3)   Flory, P.J. *Principles of Polymer Chemistry*. **1953,** Cornell University Press; New York.

(4)   Lynch, I.; and Dawson, K.A. *Macromol. Chem. Phys.* **2003**, *204*, 443-450.

(5)   Zhang, X.Z.; and Zhuo, R.X. *Eur. Polym. J.* **2000**, *36*, 2301-2303.

(6)   Flores-Flores, C.; Martinez, A.; Munoz-Dlegado, E.; and Vidal, C.J. *Biochem. Biophys. Res. Comm.* **1996**, *53-58.*

(7)   Cauet, G.; Friboulet, A.; and Thomas, D. *Biochim. Biophysic. Acta.* **1987**, *912*, 338-342.

(8)   Massoulié, J.; and Bon, S. *Ann. Rev. Neurosci.* **1982**, *5*, 57-106.

(9)   Almon, R.R.; Andrew, C.G.; and Appel, S.H. *Biochem.* **1974**, *13*, 5522-5528.

(10)  Mallender, W.D.; Szegletes, T.; and Rosenberry, T.L. *J. Biol. Chem.* **1999**, *274*, 8491-8499.

(11) Rosenberry, T.L.; and Bernhard, S.A. *Biochem.* **1972**, *11*, 4308-4321.

(12) Malany, S.; Sawai, M.; Sikorski, R.S., Seravalli, J.; Quinn, D.M.; Radic, Z.; Taylor, P., Kronman, C.; Velan, B.; and Shafferman, A. *J. Am. Chem. Soc.* **2000**, *122*, 2981-2987.

(13) Lee, K.; and Asher, S.A. *J. Am. Chem. Soc.* **2000**, *122*, 9534-9537.

(14) Rosenfeld, C.A.; and Sultatos, L.G. *Toxicol. Sci.* **2006**, *90*, 460-469.

(15) Huglin, M.B.; and Yip, D.C. *Macromolecules.* **1992**, *25*, 1333-1337.

(16) Peppas, N.A.; and Khare, A.R. *Adv. Drug Deliv. Rev.* **1993**, *11*, 1-35.

(17) Martin, J. E.; Wilcoxon, J.; and Odinek, J. *Phys. Rev. A*, **1991**, *43*, 858-872.

(18) Kaneo, Y.; Hashihama, S.; Kakinoki, A.; Tanaka, T.; Nakano, T.; and Ikeda, Y. *Drug Metab. Pharmacokinet.* **2005**, *20*, 435-442.

(19) Paradossi, G.; Cavalieri, F.; Chiessi, E.; Spagnoli, C.; and Cowman, M.K. *J. Mat. Sci. Mat. In Med.* **2003**, *14*, 687-691.

(20) Chatterjee, J.; Haik, Y.; and Chen, C.J. *BioMag. Res. Tehcnol.* **2004**, *2*, 2-4.

(21) Marouka, S.; Matsuura, T.; Kawasaki, K.; Okamoto, M.; Yoshiaki, H. *Curr. Eye Res.* **2006**, *31*, 599-606.

(22) Pal, K.; Banthia, A.K.; and Majumdar, D.K. *J. Biomat. Appl.* **2006**, *21*, 75-91.

(23) Bajpai, A.K.; and Saini, R. *Polym. Inter.* **2005**, *54*, 1233-1242.

(24) Searle, P.L. *Analyst*, **1984**, *109*, 549-568.

(25) Harfmann, R.G.; and Crouch, S.R. *Talanta,* **1989**, *36*, 261-269.

(26) Juttner, F. *Fres. J. Anal. Chem.* **1999**, *363*, 128-129.
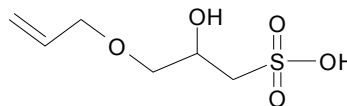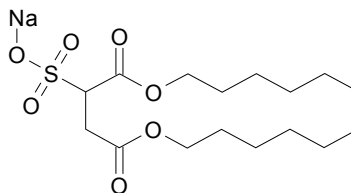
# APPENDIX: Colloidal Particle Synthesis Chemical Structures

Styrene
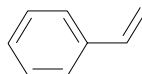
Divinyl Benzene

COPS-I

MA-80-1

Sodium Persulfate